UNIVERSITÀ DEGLI STUDI DI NAPOLI FEDERICO II

SCUOLA DI MEDICINA E CHIRURGIA

Dipartimento di Scienze Biomediche Avanzate

Direttore Prof. Alberto Cuocolo

DOTTORATO DI RICERCA IN SCIENZE BIOMORFOLOGICHE E CHIRURGICHE

XXXIII CICLO

Coordinatore Prof. Alberto Cuocolo

TESI DI DOTTORATO

THE ROLE OF IMAGING BIOMARKERS DERIVED FROM PET/CT STUDIES IN DIAGNOSIS, THERAPY AND PROGNOSIS OF CANCER PATIENTS

RELATORE

Ch.ma Prof.ssa Silvana Del Vecchio

CANDIDATO

Dott.ssa Sara Pellegrino

CONTENTS

1 INTRODUCTION

1.1 Imaging biomarkers

Daily clinical practice in oncology requires the use of a number of biomarkers for the accurate management of cancer patients. These biomarkers can be derived from molecular, histological or biochemical analysis of patients' specimens or can be obtained from measurements made on medical images. The first class of biomarkers includes molecules such as proteins, DNA, RNA or even pool of genes that can determine the risk to develop cancer, predict cancer recurrence or response to therapy in a given patient and monitor disease progression. For instance, EGFR mutational status in non-small cell lung cancer (NSCLC) predicts response to therapy with EGFR tyrosine kinase inhibitors; PSA levels allow to monitor disease progression in patients with prostate cancer; expression of estrogen and progesteron receptors along with HER2 levels guides treatment decisions in patients with breast cancer. Therefore, according to the definition proposed by the Biomarkers Definitions Working Group (1), a biomarker of this class is "a characteristic that is objectively measured and evaluated as an indicator of normal biological processes, pathogenic processes or pharmacologic responses to a therapeutic intervention", However, many treatment decisions in cancer patients are based on imaging findings that contribute for instance to the definition of clinical TNM stage, the evaluation of tumor response and the stratification of risk of recurrence. Therefore, the current FDA-NIH biomarker Working Group definition includes molecular, histological, "radiographic" and physiologic characteristics in the list of biomarkers (2). The technological evolution of imaging instrumentations and the continuous progress in image processing increased the number of imaging biomarkers and they are currently defined as features derived from one or more medical images (2). All imaging modalities including positron emission tomography (PET) / Computed Tomography (CT), Magnetic Resonance Imaging (MRI), Computed Tomography (CT) can allow the

identification and quantitative evaluation of imaging biomarkers (3). When validated, they can be used in the diagnosis, staging, prognosis and evaluation of treatment response of cancer patients (3). For these reasons, identification, quantitation and validation of imaging biomarkers became a research priority in oncological imaging (4).

1.2 PET/CT imaging modality

PET/CT is a non-invasive imaging modality that allows to visualize many biological processes in the human body (5) including metabolism, proliferation, hypoxia and receptor expression and provides both qualitative and quantitative parameters that can guide therapeutic decisions in cancer patients.

A number of PET tracers have been developed and used in clinical trials and in daily practice. Among these tracers, 18F-labeled 2-deoxy-D-glucose (18F-FDG), a radiolabeled glucose analogue, is the most widely used in cancer patients. The rationale to use 18F-FDG PET/CT in the detection of tumor sites relies on the fact that many malignancies have an oncogene-driven glycolytic phenotype that implies a high glucose demand due to an inefficient energy production and the consequent dependence of cancer cells from blood glucose supply (6). In fact, 18F-FDG uptake correlates with the rate of glycolysis, which is known to be markedly higher in tumors than in normal tissues (7). Therefore, 18F-FDG PET/CT is used to detect tumor lesions and to assess their aggressiveness throughout the body identifying primary tumors, lymph node involvement and metastatic lesions thus contributing to both diagnosis and staging. Moreover, 18F-FDG PET/CT can be helpful in cancer patients for restaging after treatment, during the follow-up to detect tumor recurrence, for the evaluation of treatment response and for radiotherapy planning (8). The rationale to use 18F-FDG PET/CT in the assessment of tumor response to therapy relies on the fact that conventional cytotoxic agents, by inducing tumor cell death, cause a reduction of cell viability and glucose demand with a consequent decrease of 18F-FDG uptake that may precede tumor shrinkage as assessed by anatomical measurements (9-15).

The widespread use of 18F-FDG PET/CT in oncological clinical practice lead indeed to substantial changes in management strategies of many tumors as a consequence of up-staging or down-staging of individual patients and recognition of responding and non responding patients treated with conventional chemotherapy regimens. Furthermore, a large body of evidences indicate that 18F-FDG PET/CT imaging findings can have a predictive and prognostic value. For instance in lymphoma patients, interim 18F-FDG PET/CT predicts tumor response at the end of therapy and subsequent clinical outcome. Therefore, in non responding patients, therapy might be adapted on the basis of imaging findings to improve the clinical outcome.

An additional field in which 18F-FDG PET/CT can be helpful is the assessment of intratumoral heterogeneity that is one of the main causes of therapeutic resistance, treatment failure and poor overall survival in cancer patients with metastatic disease (16-18). Heterogeneity of 18F-FDG uptake within tumors has been attributed to several factors such as cellularity, proliferation, angiogenesis, necrosis and hypoxia that have been independently associated with more aggressiveness, poorer response to treatment and worse prognosis (19). Therefore, measuring tumor heterogeneity could be extremely useful to characterize tumor aggressiveness and to select risk-adapted therapy in individual patients. In this field, texture analysis is emerging as a new tool for assessing intratumoral heterogeneity allowing the extraction of texture features from different imaging modalities, such as CT, PET/CT and MRI. This technique refers to a number of mathematical methods that may be applied to describe the relationships between the grey level intensity of pixels or voxels and their position within an image (19).

Among currently available PET radioligands, 68Ga-DOTA-conjugated somatostatin analogues, that specifically bind to somatostatin receptors (SSTR), are employed in the management of patients with neuroendocrine tumors. The rationale to use these tracers relies on the fact that well-differentiated neuroendocrine tumors (NETs) usually express high

levels of somatostatin receptors. In fact, 68Ga-labelled somatostatin analogues PET/CT shows a high sensitivity for the detection of most types of NETs, depending on the density of SSTR. The primary indication of 68Ga-DOTA-peptides PET/CT imaging is the detection and follow-up of well-differentiated NETs arising in any anatomic site (20,21). Moreover, this imaging modality can be used for monitoring disease during and after different types of treatment including surgery, radiotherapy, somatostatin analogues, chemotherapy or peptide receptor radionuclide therapy, PRRT.

PRRT employs somatostatin analogues labeled with beta-emitting nuclides to treat patients with well-differentiated NETs (22). Patient eligibility for PRRT is determined by showing the avidity of the tumor for SSTR-based radioligands. Therefore 68Ga-peptides PET/CT is performed in patients with NETs to assess SSTR expression level (23-26). Recently, several studies have evaluated the prognostic role of imaging biomarkers derived from 68Ga-peptides PET/CT studies performed in patients candidate to PRRT (27) and their potential application in the evaluation of PRRT response and in the prediction of outcome (28).

Several imaging biomarkers can be obtained from PET/CT studies and based on the tracer used, method of extraction and robustness of measurements they can be applied in different phases of cancer patient management.

1.3 Imaging parameters derived from PET/CT studies

1.3.1 Standardized Uptake Value (SUV)

The standardized uptake value (SUV) is the most frequently used semiquantitative parameter derived from 18F-FDG PET/CT studies. SUV is determined by measuring the activity within a region of interest (ROI) normalized for the injected activity and patient's body weight and represents the avidity of the tumor for FDG or for a different tracer. The value of SUV is usually reported as the mean (SUVmean) or maximum SUV (SUVmax) of all voxels within the ROI. SUVmax indicates the highest FDG uptake in a single voxel within a ROI and is currently the most commonly used parameter to estimate the metabolic activity of a

lesion being easy to calculate and operator independent. A major limitation of this PET-based parameter is that it provides a semiquantitative estimate of FDG activity in a single voxel of a tumor lesion and therefore it may not be representative of the metabolic degree of the whole tumor. A third SUV measurement, SUVpeak, is defined as the average SUV within a small, fixed-size ROI (ROIpeak) centered on a region of the tumor with a high tracer uptake.

To achieve more accurate and reproducible measurement of SUV, different normalization methods have been proposed (29). In addition to normalization for injected dose and body weight, normalization for lean body mass, body surface area or a combination of body weight and plasma glucose levels have been used (29). Among these normalization methods, SUV corrected for lean body mass (SUL) has been selected for treatment evaluation according to recent guidelines for the assessment of tumor response with PET (PERCIST) (30). SUV is subjected to several sources of confounders including biological and technological factors (31). Biological factors, such as patient blood glucose levels, time after tracer injection and respiratory motion, can have impact on SUV measurements. For instance, plasma glucose levels are known to cause a significant reduction in tumor FDG uptake and consequently a reduction in SUV (32). Moreover, even technological factors such as ROI drawn on the images, interscanner variability in image acquisition and reconstruction parameters can make a substantial difference (33). Therefore, variations in body composition and injected dose, differences in scanner hardware and reconstruction methods are important sources of variation with great impact on generated SUV. To overcome these limitations, achieve more accurate measurement of SUV and allow reliable comparison of SUV values among patients or even in the same patient before and after therapy, it is recommended to perform PET/CT scan on the same scanner using the same imaging protocol and reconstruction methods.

1.3.2 Metabolic Tumor Volume (MTV) and Total Lesion Glycolysis (TLG)

Metabolic Tumor Volume (MTV) and Total Lesion Glycolysis (TLG) are volumetric imaging parameters derived from 18F-FDG PET/CT study that have been proposed for metabolic stratification of cancer patients. While SUVmax is a single voxel value, MTV and TLG represent three-dimensional parameters including information on both tumor burden and metabolic activity. MTV represents the volume inside an operator- or algorithm-defined ROI that segments the metabolically active part of the tumor. TLG is calculated as the product of MTV and the correspondent value of SUVmean. Moreover, MTV and TLG can be determined not only in primary tumors but also in lymph nodes and metastatic lesions thus providing the total metabolic tumor burden of each patient. The sum of MTV and TLG of all lesions in a patient will reflect the volumetric extension of metabolically active disease and the aggressiveness of the tumor.

Several methods have been proposed for delineating tumor boundaries on PET images, using manual, semiautomatic and automatic approaches (34-38). Tumor borders can be manually drawn by a nuclear medicine physician, a radiologist, or a radiation oncologist based on visual perception of the tumor border and the volume of that region is calculated to obtain MTV (39).

Alternatively, tumor borders can be delineated by automatic or semiautomatic methods using a fixed pre-defined threshold and all voxels with SUV above the threshold are assigned to tumor and all SUV below the threshold are considered part of the background. The threshold can be an absolute SUV value (fixed absolute threshold) or can be expressed as a percentage of SUVmax within the tumor (fixed relative threshold). Among fixed absolute thresholds, the most widely accepted threshold is a SUV value of 2.5 based on the assumption that background activity is around that value in 18F-FDG PET/CT studies (40). When using a relative fixed threshold, the most common threshold chosen for tumor delineation is 40-43% of SUVmax (41).

Moreover, a background threshold method has been proposed. Using this method, a ROI is drawn in the liver or in the mediastinal blood pool and then background SUV is measured. Generally, the threshold is defined as SUV mean plus 1 or 2 standard deviation (SD) of the background (42,43). More advanced algorithm-based methods have been developed to delineate tumor borders. Among them, gradient-based methods define tumor borders by exploiting the image gradient that exists between the high SUV in tumor cells and the lower SUV in adjacent non-tumor tissues (44). Other algorithm-based methods include classifier-based methods and statistical methods. In particular, fuzzy c-means (FCM) algorithm and fuzzy locally adaptive Bayesian (FLAB) algorithm have been used in many types of malignancies (45,46).

To date, despite the exploitation of several segmentation methods, a standardization has not been achieved yet and more validation studies are needed. Nevertheless, MTV was found to be a strong predictor of prognosis irrespective of the method used for its measurement in many types of tumors (47,48).

1.3.3 Receptor Expressing Tumor Volume (RETV) and Total Lesion Receptor Expression (TLRE)

Receptor Expressing Tumor Volume (RETV) and Total Lesion Receptor Expression (TLRE) are volume-based imaging parameters equivalent to MTV and TLG but derived from 68Ga-DOTA-conjugated peptides PET/CT. They reflect not only SSTR expression but also tumor volume in NET lesions. Tumor borders visualized on 68Ga-peptides PET images can be delineated using a fixed pre-defined threshold or by using algorithm-based methods (49-51) and RETV can be calculated as the volume of this delineated tumor whereas TLRE is calculated by multiplying RETV by SUVmean of the delineated lesion.

Currently, as for MTV and TLG, there is no consensus about how to delineate RETV and TLRE and further studies are needed to achieve a standardization.

2 AIM AND STRUCTURE OF THE THESIS

The aim of the thesis was to analyze PET/CT studies performed with 18F-FDG or 68Ga-DOTA-TOC in different groups of cancer patients in order to derive imaging biomarkers and to test their role in the diagnosis, evaluation of treatment response and prognosis of various types of malignancies.

Following a general description of the materials and methods, the result's section includes several chapters and each of them will provide an overview of the study conducted in each group of patients with non-small cell lung cancer, multiple myeloma and lymphoma, thymic epithelial tumors and neuroendocrine tumors.

3 MATERIALS AND METHODS

3.1 18F-FDG PET/CT study and image analysis

18F-FDG PET/CT scans were acquired after fasting for 8 h and 60 min after intravenous administration of 18F-FDG (370 MBq). Hybrid imaging was performed using a PET/CT Discovery LS scanner (GE Healthcare, Chicago, IL, USA). CT scan was acquired using the following parameters: 4 × 5 mm collimation (140 kV, 80 mAs), 0.8 s rotation time, pitch of 1.5; a fully diagnostic contrast-enhanced CT was acquired if not previously performed. PET scan was performed in 2-dimensional mode using 4 min per bed position and six to eight bed positions per patient, depending on patient height. Iterative images reconstruction was completed with an ordered subsets-expectation maximization algorithm (2 iterations, 28 subsets). Attenuation corrected emission data were obtained using filtered back projection of CT reconstructed images (Gaussian filter with 8 mm full width half maximum) to match the PET resolution. CT and PET images were matched and fused into transaxial, sagittal, and coronal images and examined and then transferred in DICOM format to a specific

workstation allowing processing and analysis of data. All areas of focal 18F-FDG uptake visible on two contiguous PET slices at least and not corresponding to physiological tracer uptake were considered to be positive. A tridimensional region of interest was drawn around each tumor lesion and all spatially connected voxels with SUV above a predefined fixed threshold were grouped. The accuracy of tumor delineation was confirmed on the corresponding CT images and then volume-based imaging parameters, such as SUVmax, SUVmean, MTV and TLG were obtained by computed analysis of each ROI.

3.2 68Ga-DOTA-conjugated peptides PET/CT study and analysis

68Ga-DOTA-conjugated peptides PET/CT scans were acquired 60 min after intravenous administration of 68Ga-peptide (mean±SD, 135±25 MBq) using an Ingenuity TF scanner (Philips Healthcare, Best, The Netherlands). CT scan was acquired using these parameters: 120 kV, 80 mA, 0.8 s rotation time, pitch of 1.5. PET scan was acquired in 3D mode, from the top of skull to the upper thigh from 6 to 8 bed positions per patient, depending on height (3 min/each bed position). Iterative reconstruction of images was performed with an ordered subsets-expectation maximization algorithm. Attenuation corrected emission data were obtained using filtered back projection of CT reconstructed images. The resulting transaxial, sagittal and coronal PET, CT and fusion images were examined using the Ingenuity TF software, then images were transferred in DICOM format to a specific workstation equipped with a program to analyze PET data. All focal areas not attributable to physiological uptake of 68Ga-peptide that showed morpho-structural alterations on the corresponding CT images were considered to be positive. In case of multiple liver or bone metastases, the lesion with the highest SUVmax was analyzed. A volume of interest (VOI) for each positive lesion was obtained by drawing a three-dimensional region around the target lesion using an automatic segmentation method that groups all spatially connected voxels within a predefined threshold. In particular, a threshold of SUV> 2.5 was used in all tumor lesions based on the mean SUVmax value of mediastinal blood pool plus 2 SD, except for liver metastases where,

due to the high physiological liver uptake, a relative threshold of 30% of the SUVmax was used to avoid the inclusion of normal parenchyma in the VOI. In addition, the accuracy of tumor segmentation was confirmed on the corresponding CT images. Volume-based imaging parameters, such as SUVmax, SUVmean, CoV (Standard Deviation divided by SUVmean), RETV and TLRE, were obtained by computed analysis of each VOI.

3.3 Statistical analysis

Statistical analysis was performed using the software MedCalc for Windows, version 10.3.2.0 (MedCalc Software, Mariakerke, Belgium). Student's t-test was used to compare means of unpaired data. A probability value of <0.05 was considered statistically significant. For survival analysis, univariate and multivariate analyses of clinical and imaging variables were performed using Cox proportional hazards regression and receiver-operating characteristic (ROC) curve analysis was performed to estimate the best discriminative value of independent prognostic variables between patients who had died and survivors and between patients with and without progression. Finally, Kaplan-Meier analysis and log-rank tests were performed. Progression-free survival (PFS) was measured from the date of the baseline 18F- FDG PET/CT to the first observation of progressive disease, relapse, or death. Overall survival (OS) was measured from the date of the baseline 18F- FDG PET/CT to the date of death.

4 RESULTS

4.1 LUNG CANCER

4.1.1 Total metabolic tumor volume by 18F-FDG PET/CT for the prediction of outcome in patients with non-small cell lung cancer (Ref. 52)

Sixty-five patients (45 men, 20 women) with histologically proven non-small cell lung cancer, who had undergone 18F-FDG PET/CT scan during initial staging before any therapy, were included in this study. These patients were in all stages of disease (18 in stage I, 4 in stage II, 14 in stage III and 29 in stage IV). MTV of each lesion was calculated from PET data using an automated contouring program setting an absolute threshold for SUVmax at 2.5. The TLG of each lesion was calculated by multiplying MTV for the correspondent value of SUVmean. Total MTV (MTV_{TOT}) and whole-body TLG (TLG_{WB}) were calculated by the sum of the corresponding values for all primary tumors, regional lymph nodes and distant metastatic lesions. A total of 298 lesions were analyzed including 65 primary tumors, 114 lymph nodes of both regional and non-regional sites and 119 distant metastases. It was possible to determine MTV and TLG in 276 out of 298 lesions, including 65 primary tumors, 100 metastatic lymph nodes and 111 distant metastases (10 contralateral lung nodules, 72 bone metastases, 6 hepatic lesions, 3 adrenal metastases and 20 lesions in other sites). Mean value of MTV_{TOT} was 81.83 ml ± 14.63 ml (standard error, SE) whereas mean value of TLG_{WB} was 459.88 g ± 77.02 g (SE) (Table 1). Figure 1 shows representative images of the ROIs drawn around primary tumor, lymph nodes and metastatic lesions in a patient with stage IVA lung adenocarcinoma. Univariate analysis showed that, among the variables tested, primary tumor diameter, MTV of primary lesion, MTV_{TOT}, TLG_{WB}, stage and treatment predicted PFS in NSCLC patients, while OS was predicted by age, MTV of primary lesion, MTV_{TOT}, TLG_{WB}, stage and treatment (Table 2). At multivariate analysis, age, TLG_{WB} and stage were retained in the model for the prediction of PFS (χ^2=38.2340, p<0.0001) while age, MTV_{TOT} and stage were retained in the model for the prediction of OS (χ^2=44.3760, p<0.0001). Following ROC curve analysis to estimate cutoff levels, survival analysis by Kaplan-Meier method and log-rank testing showed that patients with $TLG_{WB} \leq 54.7$ g had a significantly prolonged PFS as compared to patients having $TLG_{WB} > 54.7$ g (χ^2=19.5414, p<0.0001) (Fig. 2a). Moreover, OS was significantly better in patients with $MTV_{TOT} \leq 9.5$ ml

as compared to those having MTV_{TOT} > 9.5 ml (χ^2=16.8284, p<0.0001) (Fig. 2b). Similar results were obtained in a subgroup of 43 patients with advanced disease (stages III and IV). In particular, in this subgroup of patients, MTV_{TOT} was found to be an independent predictor of both PFS and OS; survival analysis showed that patients with MTV_{TOT} ≤ 81.6 ml had a PFS significantly longer than that of patients having MTV_{TOT} > 81.6 ml (χ^2=8.5297, p=0.0035) (Fig. 3a). Similarly, OS was significantly better in patients with MTV_{TOT} ≤ 100.2 ml as compared to those with MTV_{TOT} > 100.2 ml (χ^2=8.3283, p=0.0039) (Fig. 3b). This study shows that MTV_{TOT} and TLG_{WB} obtained from 18F-FDG PET/CT are able to predict clinical outcome in patients with NSCLC. In particular, MTV_{TOT} can be used as a prognostic parameter for OS in NSCLC patients in all stages of disease independently from other established prognostic factors while TLG_{WB} is an independent predictor of PFS in the same patients. Furthermore, in a subgroup of 43 patients with advanced disease, MTV_{TOT} was found to be an independent predictor of both PFS and OS indicating that this parameter may contribute to the further prognostic stratification of NSCLC patients in the same stage, allowing risk-adapted therapy in individual patients.

Our findings taken together indicate that volume-based PET parameters are reliable predictors of PFS and OS in NSCLC patients independently from the stage and they may be employed for adaptation of therapy in individual patients.

4.1.2 PET-Based Volumetric Biomarkers for Risk Stratification of Non-Small Cell Lung Cancer Patients (Ref. 53)

This article provides an overview of the studies showing the prognostic and predictive role of MTV and TLG in NSCLC patients and evaluating the role of MTV and TLG in the new era of immunotherapy in lung cancer. Among studies evaluating MTV and TLG measured only in primary tumors of NSCLC patients (Table 3), a meta-analysis by Liu et al (54), including 5807 patients, showed that higher values of SUVmax, MTV and TLG predicted a higher risk

of disease recurrence or death in patients who were candidates to surgery. The authors suggested the usefulness of 18F-FDG PET/CT to select patients with higher risk of disease recurrence or death that may benefit from additional treatment. In another study, Anwar et al (55) studied 49 patients with stage I NSCLC who underwent 18F-FDG PET/CT at baseline and then were subjected to complete surgical resection of the tumor. PET/CT scans of these patients were analyzed in order to obtain imaging parameters capable of identifying patients at high risk of recurrence thus requiring further post-operative treatment. Their findings showed that baseline SUVmax, MTV and TLG were statistically significant prognostic factors in completely resected stage I NSCLC. Moreover, MTV was more accurate than SUVmax in predicting recurrence with 89% sensitivity and 73% specificity. Another study conducted by Dosani et al (56) included 134 patients with inoperable early stage NSCLC treated using stereotactic ablative radiotherapy with curative intent. In this patient cohort, MTV appeared to be a prognostic factor of local control (LC) and OS. In fact, when patients were dichotomized into low-MTV and high-MTV subgroups based on the median MTV of 2.4 ml, those with MTV higher than the median value had worse outcome compared to patients having MTV lower than this cutoff (26.9 vs 48.3 months). Furthermore, other studies evaluated the predictability of occult lymph node metastasis (OLM) using metabolic parameters on pretreatment 18F-FDG PET/CT (57,58); for instance, in the study conducted by Kim et al (57) 63 patients with squamous cell NSCLC clinically node-negative before surgery were enrolled and volume-based PET parameters were obtained. At multivariate analysis, high values of SUVmax and MTV showed an association with an increased risk of OLM. Moreover, ROC curve analysis showed that AUC of MTV (AUC 0.758) for the prediction of OLM was higher as compared to AUCs of SUVmax (AUC 0.712) and TLG (AUC 0.737). Additional studies evaluated volume-based PET parameters changes during treatment and their ability to predict clinical outcome in NSCLC patients (59,60). Roengvoraphoj et al. (59) studied 65 patients with inoperable locally advanced NSCLC

(stage IIIA/B) treated with definitive chemoradiotherapy in order to evaluate the role of MTV changes before, during, and after chemoradiotherapy (CRT) in primary tumors. Their findings showed that patients with pre-MTV >63 cm^3 and those with post-MTV >25 cm^3 both had significantly worse outcome.

Among studies evaluating the prognostic role and the stratification power of total or whole-body MTV or TLG (Table 4), Bazan et al (61) showed that pretreatment whole-body MTV was an independent predictive factor of OS in a cohort of uniformly treated patients with stage III NSCLC. Another study including only NSCLC patients in stage III evaluated the usefulness of whole-body MTV to stratify patients for the adoption of the most appropriate therapeutic strategy (62). Their findings showed that PET parameters may help to choose whether a patient in stage IIIA should receive a more aggressive treatment as that for stage IIIB or a less intensive regimen as that for stage IIB. Chen et al (63) evaluated the prognostic role of whole-body TLG in 105 NSCLC patients in all stages of disease; their results showed that whole-body TLG could be a promising tool for patients stratification achieving risk-adapted therapies. Additional studies evaluated whole-body volume-based PET parameters changes during treatment testing their ability to predict outcome in NSCLC patients. A study conducted by Chen et al (64), indeed, evaluated the prognostic role of volumetric metabolic parameters measured during and after radiation-based therapy in stage III NSCLC patients. In their study, ΔTLG and ΔMTV, especially ΔTLG, determined during RT had prognostic value demonstrating that 18F-FDG PET/CT scan performed during RT could be more useful than post RT 18F-FDG PET/CT scan for risk stratification.

In the new era of immunotherapy, many studies evaluated the potential role of volume-based PET parameters in NSCLC patients subjected to immunotherapy (65-70). For instance, Kaira et al (65) evaluated in their prospective study the role of volumetric parameters obtained from 18F-FDG PET/CT scans in predicting tumor response to nivolumab in NSCLC patients. 18F-FDGPET/CT of 24 patients enrolled in the study was performed before and 1

month after nivolumab administration and SUVmax, MTV, and TLG were calculated on PET images. They demonstrated that metabolic response assessed as changes of volumetric parameters (especially TLG) was closely associated with therapeutic response and survival after nivolumab administration.

4.1.3 Heterogeneity of glycolytic phenotype in advanced NSCLC (manuscript in preparation)

Eighty-four NSCLC patients (59 men, 25 women) with advanced disease (stages III and IV) who had undergone whole-body 18F-FDG PET/CT before any therapy at our Institution were enrolled in this study. Among all patients, 28 patients were in stage III (7 IIIA, 11 IIIB and 10 IIIC) while 56 patients were in stage IV (19 IVA and 37 IVB). To obtain volume-based PET parameters, a VOI of each lesion was delineated on PET images by drawing a tridimensional region around the target lesion using an automated contouring program setting an absolute threshold for SUVmax at 2.5, in agreement with previous studies (71). By computed analysis of each VOI the following parameters were obtained: SUVmean, SUVmax, MTV, TLG and Coefficient of Variation (CoV, i.e. SD divided by SUVmean). Among the texture features for the assessment of tumor heterogeneity, CoV is a simple and easy to calculate first order parameter that indicates the percent variability of SUVmean within the tumor volume reflecting the heterogeneity of glycolytic phenotype. Moreover, MTV_{TOT} and TLG_{WB} were calculated by the sum of the corresponding values for all primary tumors, lymph nodes and distant metastases; in particular, a total of 417 lesions were analyzed including 82 primary tumor lesions, 163 lymph nodes (132 regional and 31 non-regional), 14 liver metastases, 105 bone lesions and 53 metastases in other sites. To evaluate the heterogeneity of glycolytic phenotype, lesions were divided into six subgroups including primary lung tumors, regional lymph nodes, non-regional lymph nodes and distant metastases (liver, bone and lesions in other sites). Then coefficient of variation was evaluated in one representative

lesion of each subgroup in all patients. In case of multiple lymph nodes, liver, bone or other distant metastases, the lesion with the highest SUVmax was evaluated for each anatomic district. Therefore, CoV was determined in a total of 194 lesions including 84 primary lung tumors, 48 regional lymph nodes, 17 non-regional lymph nodes, 9 liver metastases, 23 bone lesions and 13 metastases in other sites. Figure 4 and Figure 5 show representative images of the ROIs drawn around primary tumor, lymph nodes and metastatic adrenal lesions in two patients with NSCLC in stage IVA. There were no statistically significant differences between mean SUVmax values of primary lesions, regional lymph nodes, non-regional lymph nodes, liver, bone and other metastases. Moreover, there were no statistically significant differences between CoV values of primary lesions, regional lymph node metastases, non-regional lymph nodes, liver, bone and other metastases.

Then survival analysis was performed including age, gender, histology, stage, MTV_{TOT}, TLG_{WB} and imaging parameters derived from 84 primary lung tumors, such as primary tumor diameter, MTV, TLG, SUVmax, SUVmean and CoV. In particular, SUVmax, SUVmean and CoV of primary tumor were dichotomized using the median value as a threshold. At univariate analysis, OS was predicted by CoV, MTV_{TOT}, TLG_{WB} and stage (Table 5). These variables along with age were tested in multivariate analysis and only age, CoV, MTV_{TOT} and stage were retained in the model (χ^2=24.4730, p=0.0001). Then Kaplan-Meier analysis and long-rank testing were performed using the median values of CoV (0.38) and MTV_{TOT} (89.5 ml) as cutoff. In particular, patients with CoV > 0.38 showed significantly better OS as compared to patients having CoV ≤ 0.38 with an OS of 18 months vs 10 months (χ^2=6.0005, p=0.0143) (Fig. 6a). Moreover, OS was significantly better in patients with MTV_{TOT} ≤ 89.5 ml than that of patients having a MTV_{TOT} > 89.5 ml with an OS of 15 months vs 7 months (χ^2=7.4546, p=0.0063) (Fig. 6b). Finally, we combined CoV and MTV_{TOT} in all possible arrangements for Kaplan-Meier analysis. Figure 7 shows survival curves in the subgroups of patients having CoV ≤ 0.38 and MTV_{TOT} > 89.5 ml, CoV ≤ 0.38 and MTV_{TOT} ≤ 89.5 ml,

CoV > 0.38 and MTV_{TOT} > 89.5 ml, CoV > 0.38 and MTV_{TOT} ≤ 89.5 ml. There was a statistically significant difference among the four survival curves (χ^2=14.1719, p=0.0027). Patients with COV ≤ 0.38 and MTV_{TOT} > 89.5 ml had the worst prognosis in terms of OS. The best OS was observed in patients with COV > 0.38 and MTV_{TOT} ≤ 89.5 ml. The other two subgroups had an intermediate pattern of survival.

PFS was significantly predicted by MTV_{TOT}, TLG_{WB}, and stage (Table 5); these variables along with age were tested in the multivariate analysis and only MTV_{TOT} and stage were retained in the model (χ^2=14.6020, p=0.0007).

Our findings indicated that a simple and easy first order volume-based PET parameter, CoV, could predict clinical outcome in NSCLC patients, thus reflecting heterogeneity of glycolytic phenotype. In particular, lower COV values predicted worse OS in these patients suggesting that a high expression of the glycolytic phenotype in a large number of tumor cells (small SD and high SUVmean) can be associated to a high aggressiveness of the disease, poor response to treatment and consequently poor prognosis.

4.1.4 Performance of FDG-PET/CT in solitary pulmonary nodule based on pre-test likelihood of malignancy: results from the ITALIAN retrospective multicenter trial (Ref. 72)

This was a multicenter study involving several PET centers in Italy. 18F-FDG PET/CT scans of 502 patients with solitary pulmonary nodule (SPN) collected from participating centers were retrospectively reviewed and analyzed. According to the Brock model of pre-test probability of lung malignancy (73), patients were stratified into low (<5%), intermediate (5-65%) and high (>65%) category risk, with a further low-risk stratification (< 10%) derived from the British Thoracic Society (BTS) (74). By the analysis of PET images, FDG uptake in SPN was assessed using not only a visual 4-point scoring system (1 = absent; 2 = mild; 3 = moderate and 4 = intense) (74) but also the ratio between the SUVmax in the SPN and

SUVmean in the mediastinal blood pool (BP) and in the liver (L). The benignity or the malignancy of SPN was established by histopathology and/or by other imaging data at follow-up. Therefore, out of 502 patients, SPN was malignant in 180 (36%), benign in 175 (35%) and indeterminate in the remaining 147 (29%). The 355 patients with a known SPN nature (malignant or benign) were considered for the analysis. At visual analysis, no FDG uptake was found in 102 patients (28.7%), while 74 (20.8%), 34 (9.6%), and 145 (40.8%) had a mild (score = 2), moderate (score = 3) and intense (score = 4) FDG uptake in the SPN respectively. Therefore, FDG uptake was higher than score 2 in 179 patients (50.4%). By referring to visual data analysis (FDG uptake ≥ 2 vs < 2), sensitivity, specificity, positive predictive value (PPV), negative predictive value (NPV) and accuracy of 18F-FDG PET/CT for the characterization of SPN were 85.6%, 85.7%, 86%, 85.2% and 85.6%, respectively.

Furthermore SUV ratios were significantly higher in patients with a malignant SPN than in those having a benign pulmonary nodule (SUVmax nodule/SUVmeanL ratio: 3.03 ± 2.16 vs 0.74 ± 0.95; SUVmax nodule/SUVmeanBP ratio: 4.08 ± 3.04 vs 0.97 ± 1.14 respectively; both $p < 0.001$). By ROC curve analysis, in all 355 patients the best cutoffs for discriminating between benign and malignant SPN were 1.56 (AUC: 0.899) and 1.12 (AUC: 0.897) for SUVmax/SUVmeanBP and SUVmax/SUVmeanL ratios, respectively. By using these cutoffs, the highest value for sensitivity and specificity was reported in patients with high likelihood of malignancy and using SUVmax nodule/SUVmeanBP ratio.

These findings showed that visual 18F-FDG PET/CT has an acceptable performance in patients with SPN, but accuracy improves when SUVratios are introduced, especially in patients with intermediate and high risk of malignancy. In particular, in high-risk patients with an indeterminate SPN, the additional information provided by the ratio between SUVmax of SPN and SUVmean of BP may significantly reduce the false positive rate associated with the visual analysis alone.

4.2 MULTIPLE MYELOMA AND LYMPHOMA

4.2.1 Visual and volumetric parameters by 18F-FDG-PET/CT: a head to head comparison for the prediction of outcome in patients with multiple myeloma (Ref. 75)

Forty-seven patients (29 males, 18 females) with untreated multiple myeloma (MM) in stage IIIA who had undergone 18F-FDG PET/CT at our Institution were enrolled in this study. To measure MTV and TLG, a 3D ROI was drawn around each target lesion throughout the whole-body and SUVmax was determined in the selected volume. In lesions showing SUVmax > 2.5, MTV was calculated grouping all spatially connected voxels within a threshold of 40% of the SUVmax, using an in-house developed SUV-based automated contouring program. The total MTV was defined as the sum of MTV values of all focal lesions selected. The TLG was obtained by multiplying the MTV of each focal lesion for the correspondent SUVmean value. The global TLG of each patient was defined as the sum of TLG values of all focal lesions selected. Moreover, visual parameters based on the Italian Myeloma Criteria for PET Use (IMPeTUs) were obtained from 18F-FDG PET/CT scan of each patients, including the metabolic state of the bone marrow according to Deauville scale (76), the presence of diffuse uptake in limbs and ribs, the site of focal PET-positive lesions, the number of focal PET-positive lesions, the metabolic state of the hottest lesion according to Deauville scale, the number of lytic lesions and, finally, the presence of extramedullary disease (nodal or extranodal), paramedullary disease, and/or fractures (Table 6). Examples of visual and volumetric parameters derived from 18F-FDG PET/CT scans obtained in the same patient are reported in Figure 8. For statistical purposes, patients showing progressive disease or dead were grouped (n=26) to be compared with those in complete or partial remission (n=21). Similarly, patients with progressive disease, partial, or complete remission were grouped as survivors (n=23) to be compared with dead (n=24). Among the values of visual parameters, only the number of lytic lesions was significantly different in patients with

progressive disease as compared with those without progression (p=0.0220) and between dead and survivors (p=0.0270). Moreover, SUVmax, MTV, and TLG values were significantly different in patients with or without progression (p=0.0400, p=0.0065, and p=0.0115, respectively) and in dead and survivors (p=0.0171, p=0.0037, and p=0.006, respectively).

At univariate analysis, hemoglobin, plasma cell concentration, β2-microglobulin, spine focal lesions, number of lytic lesions, MTV and TLG predicted PFS while only MTV and hemoglobin were retained in the model in multivariate analysis. Following ROC curve analysis to estimate cutoff levels, survival analysis by Kaplan-Meier method and log-rank testing showed that PFS was significantly prolonged in patients with MTV ≤ 39.4 ml as compared with that of patients having MTV > 39.4 ml (χ^2=12.49, p=0.0004) (Fig. 9a). Similarly, patients with hemoglobin levels higher than the median value 12.8 g/dL had a significantly better PFS than those having hemoglobin ≤ 12.8 g/dL (χ^2=4.74, p=0.0294) (Fig. 9b). Moreover, in patients with hemoglobin ≤ 12.8 g/dL, PFS was significantly prolonged in patients with MTV lower than the cutoff of 39.4 ml (χ^2=6.735, p=0.0095).

At univariate analysis for OS, hemoglobin, plasma cell concentration, β2-microglobulin, SUVmax, spine focal lesions, number of lytic lesions, MTV, and TLG were all predictive of OS while only MTV and hemoglobin were retained in the model in the multivariate analysis (χ^2=11.87, p=0.0026). By Kaplan-Meier method and log-rank test, OS was significantly prolonged in patients with MTV ≤ 39.4 ml as compared with that of patients with MTV > 39.4 ml (χ^2=15.26, p=0.0001) (Fig. 10a). Similarly, patients with hemoglobin > 12.8 g/dL had a significantly better OS than those having hemoglobin ≤ 12.8 g/dL (χ^2=4.48, p=0.0342) (Fig. 10b). Moreover, in patients with hemoglobin ≤ 12.8 g/dL, OS was significantly better in patients showing MTV lower than the cutoff of 39.4 ml (χ^2=8.73, p=0.0031). This study demonstrated that MTV can be used in the prediction of PFS and OS of multiple myeloma

patients and its combination with a classical hematological parameter, hemoglobin levels, can achieve a better prognostic stratification of these patients.

4.2.2 2-deoxy-2-[18F]fluoro-D-glucose positron emission tomography/computed tomography in primary extranodal lymphomas: treatment response evaluation and prognosis (Ref. 77)

Fifty-six patients (32 men, 24 women) with primary extranodal lymphoma (PEL) who had undergone 18F-FDG PET/CT examination at the time of diagnosis (PET-I) at our Institution were included in this study; moreover, 50 of these patients (28 men and 22 women) were subjected to PET/CT scan also 30 ± 5 days after the end of chemotherapy (PET-II). The primary sites of disease were: stomach (21 patients), bone (5 patients), orbit (5 patients), soft tissue/skin (5 patients), parotid gland (4 patients), liver (4 patients), lung (4 patients), bowel (2 patients), breast, lacrimal gland, rhino-pharynx, esophagus, kidney and spleen (6 patients, 1 for each site). According to Ann Arbor staging system, 47 patients were in stage IE and 9 in stage IVA due to bone marrow involvement. To perform the analysis of data derived from PET images, focal lesions were defined as identifiable masses ≥ 1 cm in minimum diameter and showing a SUVmax ≥ 2.5. Metabolic response of PEL patients was assessed by using the Deauville five point scale (5-PS) and the Lugano classification (78). Moreover, the percentage of SUVmax reduction or increase between PET-I and PET-II studies (ΔSUVmax) was calculated and a cut-off value of 66% according to Itti et al. (79) was used to further discriminate responders from non responders. Among the 56 PEL patients, PET-I scan was positive in 50 of them (89%). At the end of treatment, using the Deauville five points scale, 37 patients had score 1, 3 patients showed score 2, 5 patients had score 3, 4 patients showed score 4 and 1 patient had score 5. According to Lugano classification, 45 patients had a complete metabolic response (CMR), 4 a partial metabolic response (PMR) and 1 a progressive metabolic disease (PMD). Moreover, among the 45

CMR patients, 41 showed a ΔSUVmax > 66% (79) whereas among the 5 non responders (4 PMR and 1 PMD), 4 patients showed a ΔSUVmax < 66%. After a mean follow-up period of 76 months, 4 patients were lost, therefore the survival analysis was performed by including the 52 remaining patients. Among these patients, 45 (86%) achieved a complete remission, 1 (2%) had a partial response, 1 (2%) relapsed and 5 (10%) patients died. For statistical purposes, patients in complete or partial remission (n=46) were grouped and compared with patients who had progressive disease or had died (n=6). At univariate analysis, PFS was predicted by age, performance status, prognostic index, ΔSUVmax and Lugano classification while at multivariate analysis, only Lugano Classification was retained in the model ($p<0.05$). By Kaplan-Meier analysis and log-rank testing, patients showing CMR had a significantly prolonged PFS as compared to patients with PMR or PMD according to Lugano classification ($p<0.01$). Univariate analysis for the prediction of OS showed that performance status, prognostic index, ΔSUVmax and Lugano classification were predictive of overall survival while only Lugano classification was retained in the model at multivariate analysis ($p<0.05$). The OS curve estimated by Kaplan-Meier method and log-rank test was significantly better in patients showing CMR as compared to patients with PMR or PMD according to Lugano classification ($p<0.01$). These findings taken together showed that 18F-FDG PET/CT could be a useful tool to evaluate treatment response and to predict clinical outcome in patients with primary extranodal lymphoma independently from other conventional reliable prognostic factors.

4.3 THYMIC EPITHELIAL TUMORS

Evaluation of metabolic response with 18F-FDG PET-CT in patients with advanced or recurrent thymic epithelial tumors (Ref. 80)

Twenty-seven patients (18 males, 9 females) with advanced (16 patients) or recurrent (11 patients) thymic epithelial tumors who had undergone 18F-FDG PET/CT before and after at least 3 cycles of standard chemotherapy regimens were enrolled in this study. From baseline 18F-FDG PET/CT scan, a total of 77 lesions were detected, including 18 mediastinal masses, 15 lymph nodes, 23 pleura/pericardial implants, 16 visceral lesions and 5 bone lesions. For the assessment of metabolic response, the lesion with the highest SUVmax value in each patient was selected as the target lesion. After treatment with standard chemotherapy, morphovolumetric tumor response was assessed by contrast-enhanced CT according to RECIST criteria (15); in particular, an objective tumor response was observed in 17 patients (2 complete response CR and 15 partial response PR) whereas in the remaining patients, 8 showed stable disease SD and 2 had progression disease PD. For statistical purposes, patients with CR and PR were grouped in the class of responders whereas patients with SD and PD were considered non responders.

SUVmax values of pre-treatment 18F-FDG PET/CT scan were not significantly different between responders and non responders (8.80 ± 5.04 vs 8.45 ± 4.88, p=0.8645) while SUVmax values of post-treatment 18F-FDG PET-CT scan were significantly lower in responders as compared to non responders (3.94 ± 3.62 vs 8.99 ± 4.34, p=0.0038).

The SUVmax value of the most metabolically active lesion in each scan was used to define the ΔSUVmax as follows: ΔSUVmax = [(SUVmax post – SUVmax pre)/SUVmax pre] × 100. The normally distributed values of ΔSUVmax were significantly different in responders and non responders (p=0.0003) and were significantly correlated with morphovolumetric response (Spearman's rank correlation, r=0.64, p=0.001). By ROC curve analysis, a ΔSUVmax value of -25% was the best discriminative value able to discriminate responders from non responders. Representative 18F-FDG PET-CT images of baseline and post-treatment scans in a patient with metabolic response and a patient with metabolic progression of the disease, respectively, were shown in Figures 11 and 12.

This study showed that metabolic response assessed by 18F-FDG PET/CT may improve current morphovolumetric criteria in the identification of responders and non responders thus providing an additional guide for adaptation of therapy in patients with advanced or recurrent thymic epithelial tumors. In particular, a 25% change of 18F-FDG uptake between baseline and post-treatment scans was able to discriminate responders from non responders and significantly correlated with tumor response assessed by RECIST criteria.

4.4 NEUROENDOCRINE TUMORS

Heterogeneity of SSTR2 expression assessed by 68Ga-DOTATOC-PET/CT using coefficient of variation in patients with neuroendocrine tumors (manuscript submitted for publication, ref. 28)

Thirty-eight patients (25 men, 13 women) with pathologically proven neuroendocrine tumors who had undergone 68Ga-DOTATOC-PET/CT scan at our Institution were enrolled in this study. Primary tumor was localized in the gastroenteropancreatic district (25 patients), in the bronchopulmonary district (7 patients) or in other anatomical districts (6 patients). Among a total of 44 gallium scans performed in these patients, 18 scans were performed in patients under treatment with somatostatin analogues using standard regimen as discontinuation of therapy was not clinically recommended. A total of 107 lesions were analyzed including 35 primary tumors (27 gastroenteropancreatic, 5 bronchopulmonary and 3 in other anatomical districts), 32 lymph nodes and 40 distant metastases (21 in the liver, 10 in the bones and 9 in other anatomical sites). For each lesion, a VOI was determined by drawing a tridimensional region around the lesion using an automatic contouring program that groups all spatially connected voxels within a predefined threshold. In particular, in all lesions was used a threshold of SUV> 2.5 based on the mean SUVmax value of mediastinal blood pool plus 2 SD, except for liver lesions where, due to the high physiological liver uptake, a

threshold of 30% of the SUVmax was used to avoid the inclusion of normal parenchyma in the VOI. By computed analysis of each VOI, the following imaging parameters were obtained: SUVmean, CoV, SUVmax, RETV and TLRE. There were no statistically significant differences between the SUVmax values in malignant lesions (primary tumors, lymph node and distant metastases) of treated and untreated patients while tracer uptake was significantly reduced in normal liver ($p<0.0001$), spleen ($p<0.0001$) and pituitary gland ($p<0.02$) of treated patients. Similarly, neither SUVmean nor CoV in primary lesions ($p=0.3515$ and $p=0.2718$, respectively), lymph node metastases ($p=0.4497$ and $p=0.0748$, respectively) and distant metastases ($p=0.1068$ and $p=0.2128$, respectively) were statistically different between treated and untreated patients. Therefore, the analysis of imaging parameters was performed in all patients as a whole group. No statistically significant differences were found between the SUVmax of primary tumors, lymph nodes and distant metastases, although the SUVmax of distant metastases tended to be higher than that of primary lesions ($p=0.0573$). There were no statistically significant differences between CoV value of primary lesions and lymph node metastases ($p=0.1730$) or distant metastases ($p=0.3260$), while lymph node metastases had a significantly higher CoV than that of distant metastases ($p =0.0253$). In a further analysis, distant metastases were divided in three subgroups including liver, bone and other metastatic lesions; bone metastases had a significantly higher CoV than both liver lesions ($p <0.0001$) and metastases of other sites ($p=0.0269$). A significant difference was also found between the CoV values of liver metastases and other metastatic lesions ($p=0.0006$). Therefore, bone lesions had the greatest heterogeneity of tracer uptake reflecting somatostatin receptor expression compared to the other distant metastases. Moreover, the CoV value of bone metastases was significantly higher than that of primary lesions ($p=0.0132$). On the other hand, liver metastases had a significantly lower CoV than that of primary lesions ($p=0.0005$) and lymph node metastases ($p=0.0001$). Finally, RETV and TLRE of distant metastases were

significantly greater than that of lymph nodes (p=0.0044 and p=0.0028, respectively) while there were no statistically significant differences between the RETV and TLRE values of primary lesions and lymph node (p=0.0879 and p=0.2616, respectively) or distant metastases (p=0.2972 and p=0.1268, respectively).

Our study showed that bone metastases had the highest CoV value followed by lymph node metastases and primary lesions reflecting the variable expression of somatostatin receptor which can depend on type and site of the lesion. These findings suggest that the biological behavior of tumor cells may vary at different sites due to receptor heterogeneity among lesions thus leading to different pattern of tumor growth, spread and response to treatment with both labeled and unlabeled somatostatin analogues.

5 DISCUSSION

PET/CT imaging modality can be used to obtain imaging biomarkers that are able to characterize tumor behavior, to predict treatment response and clinical outcome in many malignancies. In lung cancer, 18F-FDG PET/CT is currently the recognized tool for clinical staging and for evaluation of treatment response. Due to the late onset of clinical symptoms, most patients are already in advanced stages at diagnosis with the presence of distant metastases and they are candidate to chemotherapy. After an initial good response to therapy, the majority of these patients will show progression and become resistant to cancer therapy. Therefore it would be helpful to identify those with higher risk of disease progression and death allowing the adoption of more aggressive therapy. To date, the most important prognostic factor remains stage of the disease at initial diagnosis that correctly predicts PFS and OS of NSCLC patients thus guiding treatment decisions. Nevertheless, a wide variation of treatment responses and overall outcomes were observed among patients within the same stage highlighting the need to obtain additional prognostic biomarkers to better stratify

patients. In our study (52) we tested whether whole-body volumetric imaging parameters derived from 18F-FDG PET/CT scans, such as MTV_{TOT} and TLG_{WB}, may predict outcome in NSCLC in all stages of disease. According to our results, MTV_{TOT} was found to be a prognostic parameter for OS in NSCLC patients independently from other established prognostic factors whereas TLG_{WB} was an independent predictor of PFS in the same patients. Moreover, in a subgroup of 43 patients with advanced disease (stage III and IV), MTV_{TOT} was able to predict both PFS and OS indicating that this parameter may contribute to the further prognostic stratification of patients in the same stage of disease. Our findings are in agreement with previous studies evaluating the prognostic value of MTV_{TOT} and TLG_{WB} in NSCLC patients as showed in our overview (53) on PET-based volumetric biomarkers for risk stratification and prediction of outcome in NSCLC patients.

Lung cancer, as many malignancies, has a glycolytic phenotype that implies a high glucose demand that is correlated with a high FDG uptake. The evaluation of intratumoral heterogeneity of glycolytic phenotype has been identified as one of the main research fields in the last years. In our study (Heterogeneity of glycolytic phenotype in advanced NSCLC, manuscript in preparation) we tested whether a simple, first order imaging feature, such as CoV, derived from 18F-FDG PET/CT scans, may predict clinical outcome in NSCLC patients in advanced disease (stage III and IV). CoV was found to be an independent predictor of OS; therefore, patients with CoV values ≤ 0.38 had a significantly worse outcome than those having COV values > 0.38. These findings suggest that a high expression of the glycolytic phenotype in a large number of tumor cells (small SD and high SUVmean) can be associated to a high aggressiveness of the disease, poor response to treatment and consequently poor prognosis. Our results are in agreement with previous study evaluating the heterogeneity of glycolytic phenotype in lung cancer and other malignancies (81,82). Lovinfosse et al (81) studied 63 patients with NSCLC treated by stereotactic body radiation therapy (SBRT) to investigate whether 18-FDG heterogeneity could predict clinical outcome.

They demonstrated that the textural feature dissimilarity, a second order feature, was a strong independent predictor of PFS and OS; survival analysis performed by Kaplan-Meyer method showed that patients with dissimilarity lower or equal than the cutoff level had a higher risk of recurrence than those having dissimilarity > cutoff level. These findings taken together underline the role of FDG heterogeneity by PET/CT scan as an imaging biomarker able to provide additional information regarding clinical outcome in cancer patients.

Bundschuh et al (82) tested the role of tumor heterogeneity in the evaluation of therapy response by analyzing pretherapeutic (baseline) 18F-FDG PET/CT, changes occurring early in the course of neoadjuvant radiation chemotherapy (nRCT) and changes between pretherapeutic and post therapeutic 18F-FDG PET/CT scans in patients with locally advanced rectal cancer. They demonstrated that tumor heterogeneity assessed by CoV showed a statistically significant predictive ability of therapy response. Responders were classified by a reduction in COV reflecting the decrease of tumor heterogeneity during nRCT. Furthermore, to test the prognostic value of CoV, survival analysis by Kaplan-Meier method showed that patients with COV < cutoff level had a worse PFS than those having COV ≥ cutoff.

At the beginning, lung cancer can appear as a solitary pulmonary nodule, that is defined radiologically as an intraparenchymal lung lesion of less than 3 cm in diameter, with no associated atelectasis or adenopathy (83-85). A SPN can be benign or malignant so its characterization is a fundamental step in the management of these patients. In our study (72) we determined the performance of 18F-FDG PET/CT for the characterization of SPN in 355 patients using both visual and semiquantitative analysis stratifying the risk of patients according to the likelihood of pulmonary malignancies. According to visual analysis, sensitivity, specificity, PPV, NPV, and accuracy of 18F-FDG PET/CT for the characterization of SPN were 85.6%, 85.7%, 86%, 85.2%, and 85.6%. Moreover the addition of semiquantitative analysis in the form of SUVratios (i.e., SUVmax nodule/SUVmean BP),

resulted in a sensitivity and a specificity of 91.3% and 100% respectively. The results of this multicenter study suggested that the diagnostic performance of PET/CT in the evaluation of SPN significantly improves by including semiquantitative imaging parameters, such as SUVmax nodule/SUVmean BP ratio, especially in patients with intermediate or high risk of malignancy.

The ability of 18F-FDFG PET/CT to predict clinical outcome and tumor response has been evaluated not only in solid tumors but also in lymphoproliferative diseases including lymphoma and multiple myeloma. In particular, multiple myeloma is a clonal plasma cell malignancy characterized by the infiltration of the bone marrow and occasionally other extra-medullary sites (86). In MM patients, 18F-FDG PET/CT allows the characterization of both skeletal and extra-skeletal disease with high sensitivity, identifying metabolically active lesions in both pre and post treatment evaluation (87). In the prognostic assessment of these patients, one of the main factors is the evaluation of the extent of disease and 18F-FDG PET/CT, being a whole-body imaging modality, can be exploited to measure the metabolic tumor burden in all lesions throughout the whole body. Nevertheless, to date, due to the different patterns of bone marrow involvement in MM (88), a standardization of 18F-FDG PET/CT reports has not been achieved yet. Recently, the IMPeTUs criteria (89-90) were developed in order to achieve harmonization of the interpretation of 18F-FDG PET/CT scans. In our study (75) we tested the contribution of visual IMPeTUs-based parameters and volume-based PET parameters such as MTV and TLG in the prediction of PFS and OS in MM patients. According to our findings, MTV was able to predict both PFS and OS in these patients thus representing the whole metabolic burden of tumor lesions and probably due to this intrinsic characteristic, it is a better prognostic index compared to visual parameters. Moreover, the combination of MTV with a classical clinical prognostic parameter such as hemoglobin level improved the prognostic stratification of MM patients thus allowing adaptation of therapy in individual patients.

In most lymphomas, 18F-FDG PET/CT represents a recognized tool in the diagnosis, evaluation of treatment response and prognosis (91-93). According to the WHO classification, PEL is defined as an isolated extranodal localization of lymphoma with or without involvement of the adjacent lymph nodes at the moment of diagnosis (94-95). By clinical presentation, the most common sites of extranodal involvement are stomach, head and neck region, lung, bone, skin and central nervous system (96,97). In our study (77) we evaluated the role of 18F-FDG PET/CT in response assessment and prognosis of PEL patients. Our results showed that 18F-FDG PET/CT is useful in the evaluation of treatment response and in the prediction of disease progression and death in PEL patients independently from other conventional prognostic factors. Previous studies (98,99) tested the prognostic role of 18F-FDG PET/CT after therapy in lymphoma patients showing long-term remission in patients with negative post-therapy 18F-FDG PET/CT findings (100,101). Accordingly, our results showed that PEL patients showing complete metabolic response based on Lugano classification had a better PFS and OS.

Functional imaging based on 18F-FDG PET/CT findings was found to be an important step in the management of patients with thymic epithelial tumors (TETs) that are rare malignancies arising in the anterior mediastinum and showing a high variable biological behavior, from benign lesions to highly aggressive carcinomas (102,103). 18F-FDG PET/CT imaging modality by its ability to identify more aggressive and invasive subtypes of TETs provides useful information for the biologically characterization of thymic masses (104-107) and for disease stage (108-111). Moreover, this imaging technique has been used to monitor the efficacy of targeted therapy in patients with advanced TETs and a reduction of 18F-FDG uptake higher than 30% closely correlated with objective tumor response (112). Since metabolic response usually precedes the morphovolumetric reduction of tumor burden assessed by RECIST criteria (15), the early detection of treatment failure may indicate the need to adopt alternative therapeutic regimens (9-11). In our study (80) we tested whether

18F-FDG PET/CT performed in patients with advanced or recurrent TETs before and after standard chemotherapy may discriminate responders from non responders and whether metabolic response correlates with morphovolumetric RECIST criteria of tumor response. According to our results, the percentage change of 18F-FDG uptake between baseline and post-treatment scans was able to discriminate responders from non responders and significantly correlated with tumor response assessed by RECIST criteria. A 25% reduction of 18F-FDG uptake, indeed, identified responders with a sensitivity of 88% and a specificity of 80%. In TETs patients, the assessment of tumor response performed using RECIST criteria has some limitation due to the difference between TETs and other solid tumors in terms of growth and dissemination patterns especially in advanced stages. Our findings suggested that 18F-FDG PET/CT scan can contribute to the prediction of tumor response in TETs patients potentially candidate to several consecutive lines of chemotherapy in order to guide subsequent therapeutic options.

Among other tracers used in clinical practice, 68Ga-DOTA-conjugates peptides are the most widely used in the characterization of neuroendocrine tumors. These neoplastic disorders are a heterogeneous group of rare malignancies arising from the diffuse neuroendocrine cell system that includes both well-differentiated NETs and poorly differentiated carcinomas. A common property of well-differentiated NETs is the overexpression of somatostatin receptors that constitute a target for therapy with unlabeled and labeled somatostatin analogues (113,114). Among SSTR subtypes, the SSTR2 receptor is the most widely distributed in normal tissues and human tumors (115). Previous studies showed that high levels of SSTR2 could predict a good response to therapy with somatostatin analogues and a prolonged survival (116,117). Nevertheless, to date, it is still unclear how the heterogeneity of SSTR2 expression within a lesion or among different lesions in the same patient may affect tumor response to therapy and clinical outcome. In our study (28) we tested the ability of a first order parameter such as CoV obtained from 68Ga-peptide PET/CT scans to

quantify the heterogeneity of SSTR2 expression within primary and metastatic lesions of NET patients. According to our findings bone metastases had the highest CoV value followed by lymph node metastases and primary lesions reflecting the variable expression of somatostatin receptors. The heterogeneity of somatostatin receptor expression among lesions can derived from the different biological behavior of tumor cells that can vary at different body sites leading to different pattern of tumor growth and progression as well as to different response to targeted therapy with somatostatin analogues. As a PET-based first order parameter, CoV, could be used to predict tumor behavior and tumor response of NET patients although other large clinical studies are needed to confirm and validate our results.

6 CONCLUSIONS

Imaging biomarkers derived from PET/CT scans can be used to characterize tumor behavior and aggressiveness, to evaluate and predict tumor response and to predict progression-free survival and overall survival in many malignancies. These imaging parameters can be introduced in the management of cancer patients to help clinicians in the prognostic stratification of these patients in order to adopt risk-adapted individual therapy and to achieve a prolonged overall survival.

7 REFERENCES

1. Biomarkers Definitions Working Group. Biomarkers and surrogate endpoints: preferred definitions and conceptual framework. *Clin Pharmacol Ther*. 2001; 69(3):89-95.

2. O'Connor JPB, Aboagye EO, Adams JE, Aerts HJWL, Barrington SF, Beer AJ et al. Imaging biomarker roadmap for cancer studies. *Nat Rev Clin Oncol*. 2017; 14(3):169-186.

3. Prescott JW. Quantitative Imaging Biomarkers: The Application of Advanced Image Processing and Analysis to Clinical and Preclinical Decision Making. *J Digit Imaging*. 2013; 26:97-108.

4. Bernsen MR, Kooiman K, Segbers M, Van Leeuwen FWB, De Jong M. Biomarkers in preclinical cancer imaging. *Eur J Nucl Med Mol Imaging*. 2015; 42:579-596.

5. Weber WA. Positron emission tomography as an imaging biomarker. *J Clin Oncol*. 2006; 24(20):3282-92.

6. De Rosa V, Iommelli F, Monti M, Mainolfi CG, Fonti R, Del Vecchio S. Reversal of Warburg Effect and Reactivation of Oxidative Phosphorylation by Differential Inhibition of EGFR Signaling Pathways in Non-Small Cell Lung Cancer. *Clin Cancer Res*. 2015; 21(22):510-20.

7. Larson SM, Schwartz LH. 18F-FDG PET as a Candidate for ‘‘Qualified Biomarker’’: Functional Assessment of Treatment Response in Oncology. *J Nucl Med*. 2006; 47(6):901-3.

8. Croteau E, Renaud JM, Richard MA, Ruddy TD, Bénard F, deKemp RA. PET Metabolic Biomarkers for Cancer. *Biomarkers in Cancer*. 2016; 8(2):61-9.

9. Juweid ME, Cheson BD. Positron-emission tomography and assessment of cancer therapy. *N Engl J Med.* 2006; 354:496-507.

10. Wahl RL, Zasadny K, Helvie M, Hutchins GD, Weber B, Cody R. Metabolic monitoring of breast cancer chemohormonotherapy using positron emission tomography: initial evaluation. *J Clin Oncol*. 1993; 11:2101-11.

11. Weber WA, Wieder H. Monitoring chemotherapy and radiotherapy of solid tumors. Eur *J Nucl Med Mol Imaging*. 2006; 33(1):27-37.

12. Kasamon YL, Wahl RL. FDG PET and risk-adapted therapy in Hodgkin’s and non-Hodgkin’s lymphoma. *Curr Opin Oncol*. 2008; 20:206-19.

13. Kasamon YL, Jones RJ, Wahl RL. Integrating PET and PET/CT into the risk-adapted therapy of lymphoma. *J Nucl Med*. 2007; 48(1):19S-27S.

14. Therasse P, Arbuck SG, Eisenhauer EA, Wanders J, Kaplan RS, Rubinstein L et al. New guidelines to evaluate the response to treatment in solid tumors. European Organization for Research and Treatment of Cancer, National Cancer Institute of the United States, National Cancer Institute of Canada. *J Natl Cancer Inst*. 2000; 92:205-16.

15. Eisenhauer EA, Therasse P, Bogaerts J, Schwartz LH, Sargent D, Ford R, et al. New response evaluation criteria in solid tumours: revised RECIST guideline (version 1.1). *Eur J Cancer*. 2009; 45:228-47.

16. Cajal SR, Sesè M, Capdevila C, Aasen T, De Mattos-Arruda L, Diaz-Cano SJ et al. Clinical implications of intratumor heterogeneity: challenges and opportunities. *J Mol Med*. 2020; 98:161-177.

17. Jamal-Hanjani M, Quezada SA, Larkin J, Swanton C. Translational implications of tumor heterogeneity. *Clin Cancer Res*. 2015; 21(6):1258-1266.

18. Marusyk A, Almendro V, Polyak K. Intra-tumour heterogeneity: a looking glass for cancer? *Nat Rev Cancer*. 2012; 12(5):323-334.

19. Chicklore S, Goh V, Siddique M, Roy A, Marsden PK, Cook GJR. Quantifying tumour heterogeneity in 18F-FDG PET/CT imaging by texture analysis. *Eur J Nucl Med Mol Imaging.* 2013; 40:133-140.

20. Bozkurt MF, Virgolini I, Balogova S, Beheshti M, Rubello D, Decristoforo C et al. Guideline for PET/CT imaging of neuroendocrine neoplasms with 68Ga-DOTA-conjugated somatostatin receptor targeting peptides and 18F-DOPA. *Eur J Nucl Med Mol Imaging*. 2017; 44:1588-1601.

21. Pavel M, Öberg K, Falconi M, Krenning EP, Sundin A, Perren A et al. Gastroenteropancreatic neuroendocrine neoplasms: ESMO Clinical Practice Guidelines for diagnosis, treatment and follow-up. *Ann Oncol*. 2020; 31:844-860.

22. Bodei L, Mueller-Brand J, Baum RP, Pavel ME, Horsch D, O'Dorisio MS et al. The joint IAEA, EANM, and SNMMI practical guidance on peptide receptor radionuclide therapy (PRRNT) in neuroendocrine tumours. *Eur J Nucl Med Mol Imaging*. 2013; 40(5):800-816.

23. Sadowski SM, Neychev V, Millo C, Shih J, Nilubol N, Herscovitch P et al. Prospective Study of 68Ga-DOTATATE Positron Emission Tomography/Computed Tomography for Detecting Gastro- Entero-Pancreatic Neuroendocrine Tumors and Unknown Primary Sites. *J Clin Oncol*. 2016; 34(6):588-596.

24. Tirosh A, Kebebew E. The utility of 68Ga-DOTATATE positron-emission tomography/computed tomography in the diagnosis, management, follow-up and prognosis of neuroendocrine tumors. *Future Oncol*. 2018; 14(2):111-122.

25. Sundin A, Arnold R, Baudin E et al. ENETS consensus guidelines for the standards of care in neuroendocrine tumors: radiological, nuclear medicine & hybrid imaging. *Neuroendocrinology*. 2017; 105(3):212-244.

26. Hicks RJ, Kwekkeboom DJ, Krenning E, Bodei L, Grozinsky-Glasberg S, Arnold R et al. ENETS consensus guidelines for the standards of care in neuroendocrine neoplasia: peptide receptor radionuclide therapy with radiolabeled somatostatin analogues. *Neuroendocrinology*. 2017; 105(3):295-309.

27. Werner RA, Lapa C, Ilhan H, Higuchi T, Buck AK, Lehner S et al. Survival prediction in patients undergoing radionuclide therapy based on intratumoral somatostatin-receptor heterogeneity. *Oncotarget*. 2017; 8:7039-7049.

28. Fonti R, Panico M, Pellegrino S, Pulcrano A, Vastarella LA, Hakkak A et al. Heterogeneity of SSTR2 expression assessed by 68Ga-DOTATOC-PET/CT using coefficient of variation in patients with neuroendocrine tumors. Manuscript submitted for publication.

29. Vriens D, De Geus-Oei LF, Van Laarhoven HW, Timmer-Bonte JNH, Krabbe PFM, Visser EP et al. Evaluation of different normalization procedures for the calculation of the

standardized uptake value in therapy response monitoring studies. *Nucl Med Commun*. 2009; 30(7):550-7.

30. Wahl RL, Jacene H, Kasamon Y, Lodge MA. From RECIST to PERCIST: Evolving Considerations for PET Response Criteria in Solid Tumors. *J Nucl Med*. 2009; 50(1):122S-50S.

31. Thie JA. Understanding the standardized uptake value, its methods, and implications for usage. *J Nucl Med*. 2004; 45(9):1431-4.

32. Lindholm P, Minn H, Leskinen-Kallio S, Bergman J, Ruotsalainen U, Joensuu H. Influence of the blood glucose concentration on FDG uptake in cancer- a PET study. *J Nucl Med.* 1993; 34(1):1-6.

33. Boellaard R, Krak NC, Hoekstra OS, Lammertsma A. Effects of noise, image resolution, and ROI definition on the accuracy of standard uptake values: a simulation study. *J Nucl Med*. 2004; 45(9):1519-27.

34. Im HJ, Bradshaw T, Solaiyappan M, Cho SY. Current Methods to Define Metabolic Tumor Volume in Positron Emission Tomography: Which One is Better? *Nucl Med Mol Imaging*. 2018; 52:5-15.

35. Geets X, Lee JA, Bol A, Lonneux M, Gregoire V. A gradient-based method for segmenting FDG-PET images: methodology and validation. *Eur J Nucl Med Mol Imaging*. 2007; 34:1427-1438.

36. Schaefer A, Kremp S, Hellwig D, Rube C, Kirsch CM, Nestle U. A contrast-oriented algorithm for FDG-PET-based delineation of tumour volumes for the radiotherapy of lung cancer: derivation from phantom measurements and validation in patient data. *Eur J Nucl Med Mol Imaging*. 2008; 35:1989-1999.

37. van Dalen JA, Hoffmann AL, Dicken V, Vogel WV, Wiering B, Ruers TJ, et al. A novel iterative method for lesion delineation and volumetric quantification with FDG PET. *Nucl Med Commun*. 2007; 28:485-493.

38. Paulino AC, Koshy M, Howell R, Schuster D, Davis LW. Comparison of CT- and FDG-PET-defined gross tumor volume in intensity-modulated radiotherapy for head-and-neck cancer. *Int J Radiat Oncol Biol Phys*. 2005; 61:1385-1392.

39. MacManus M, Nestle U, Rosenzweig KE, Carrio I, Messa C, Belohlavek O. Use of PET and PET/CT for radiation therapy planning: IAEA expert report 2006-2007. *Radiother Oncol.* 2009; 91:85-94.

40. Fonti R, Conson M, Del Vecchio S. PET/CT in radiation oncology*. Semin Oncol*. 2019; 4:202-209.

41. Foster B, Bagci U, Mansoor A, Xu Z, Mollura DJ. A review on segmentation of positron emission tomography images. *Comput Biol Med*. 2014; 50:76-96.

42. Han EJ, Yang YJ, Park JC, Park SY, Choi WH, Kim SH. Prognostic value of early response assessment using 18F-FDG PET/CT in chemotherapy-treated patients with non-small-cell lung cancer. *Nucl Med Commun*. 2015; 36:1187-1194.

43. Hyun SH, Choi JY, Kim K, Kim J, Shim YM, Um SW, et al. Volume-based parameters of (18)F-fluorodeoxyglucose positron emission tomography/computed tomography improve outcome prediction in early-stage non-small cell lung cancer after surgical resection*. Ann Surg*. 2013; 257:364-370.

44. Graves EE, Quon A, Loo BWJ. RT_Image: an open-source tool for investigating PET in radiation oncology*. Technol Cancer Res Treat*. 2007; 6:111-121.

45. Lapuyade-Lahorgue J, Visvikis D, Pradier O, Cheze Le Rest C, Hatt M. SPEQTACLE: An automated generalized fuzzy C-means algorithm for tumor delineation in PET. *Med Phys*. 2015; 42:5720-5734.

46. Hatt M, Cheze le Rest C, Descourt P, Dekker A, De Ruysscher D, Oellers M et al. Accurate automatic delineation of heterogeneous functional volumes in positron emission tomography for oncology applications*. Int J Radiat Oncol Biol Phys*. 2010; 77:301-308.

47. Barrington SF, Meignan M. Time to Prepare for Risk Adaptation in Lymphoma by Standardizing Measurement of Metabolic Tumor Burden. *J Nucl Med*. 2019; 60:1096-1102.

48. Gallamini A. In Search of Platinum Meter Bar for Measurement of Metabolic Tumor Volume in Lymphoma. *J Nucl Med*. 2019; 60:1094-1095.

49. Toriihara A, Baratto L, Nobashi T, Park S, Hatami N, Davidzon G et al. Prognostic value of somatostatin receptor expressing tumor volume calculated from 68Ga-DOTATATE PET/CT in patients with well-differentiated neuroendocrine tumors. *Eur J Nucl Med Mol Imaging*. 2019; 46:2244-2251.

50. Liberini V, Rampado O, Gallio E, De Santi B, Ceci F, Dionisi B et al. 68Ga-DOTATOC PET/CT-Based radiomic analysis and PRRT outcome: a preliminary evaluation based on an exploratory radiomic analysis on two patients. *Front Med*. 2021; 7:601853.

51. Tirosh A, Papadakis GZ, Millo C, Hammoud D, Sadowski SM, Herscovitch P et al. Prognostic Utility of Total 68Ga-DOTATATE-Avid Tumor Volume in Patients with Neuroendocrine Tumors. *Gastroenterology*. 2018; 154(4):998-1008.

52. Pellegrino S, Fonti R, Mazziotti E, Piccin L, Mozzillo E, Damiano V, Matano E, De Placido S, Del Vecchio S. Total metabolic tumor volume by 18F-FDG PET/CT for the prediction of outcome in patients with non-small cell lung cancer. *Ann Nucl Med*. 2019; 33:937-944.

53. Pellegrino S, Fonti R, Pulcrano A, Del Vecchio S. PET-Based Volumetric Biomarkers for Risk Stratification of Non-Small Cell Lung Cancer Patients. *Diagnostics.* 2021; 11(2):210.

54. Liu J, Dong M, Sun X, Li W, Xing L, Yu J. Prognostic Value of 18F-FDG PET/CT in Surgical Non-Small Cell Lung Cancer: A Meta-Analysis. *PLoS ONE*. 2016; 11, e0146195.

55. Anwar H, Vogl TJ, Abougabal MA, Grunwald F, Kleine P, Elrefaie S et al. The value of different (18)F-FDG PET/CT baseline parameters in risk stratification of stage I surgical NSCLC patients. *Ann Nucl Med*. 2018; 32:687-694.

56. Dosani M, Yang R, McLay M, Wilson D, Liu M, Yong-Hing CJ et al. Metabolic tumour volume is prognostic in patients with non-small-cell lung cancer treated with stereotactic ablative radiotherapy. *Curr Oncol*. 2019; 26, e57-e63.

57. Kim DH, Song BI, Hong CM, Jeong SY, Lee SW, Lee J et al. Metabolic parameters using (1)(8)F-FDG PET/CT correlate with occult lymph node metastasis in squamous cell lung carcinoma. *Eur J Nucl Med Mol Imaging*. 2014; 41:2051-2057.

58. Park SY, Yoon JK, Park KJ, Lee SJ. Prediction of occult lymph node metastasis using volume-based PET parameters in small-sized peripheral non-small cell lung cancer. *Cancer Imaging*. 2015; 15:21.

59. Roengvoraphoj O, Wijaya C, Eze C, Li M, Dantes M, Taugner J et al. Analysis of primary tumor metabolic volume during chemoradiotherapy in locally advanced non-small cell lung cancer. *Strahlenther Onkol*. 2018; 194:107-115.

60. Roengvoraphoj O, Eze C, Wijaya C, Dantes M, Taugner J, Tufman A et al. How much primary tumor metabolic volume reduction is required to improve outcome in stage III NSCLC after chemoradiotherapy? A single-centre experience. *Eur J Nucl Med Mol Imaging*. 2018; 45(12):2103-2109.

61. Bazan JG, Duan F, Snyder BS, Horng D, Graves EE, Siegel BA et al. Metabolic tumor volume predicts overall survival and local control in patients with stage III non-small cell lung cancer treated in ACRIN 6668/RTOG 0235. *Eur J Nucl Med Mol Imaging*. 2017; 44:17-24.

62. Finkle JH, Jo SY, Ferguson MK, Liu HY, Zhang C, Zhu X et al. Risk-stratifying capacity of PET/CT metabolic tumor volume in stage IIIA non-small cell lung cancer. *Eur J Nucl Med Mol Imaging*. 2017; 44:1275-1284;

63. Chen HH, Chiu NT, Su WC, Guo HR, Lee BF. Prognostic value of whole-body total lesion glycolysis at pretreatment FDG PET/CT in non-small cell lung cancer. *Radiology*. 2012; 264:559-566;

64. Chen HHW, Su WC, Guo HR, Lee BF, Chiu NT. Prognostic value of volumetric metabolic parameter changes determined by during and after radiotherapy-based (18) F-FDG PET/CT in stage III non-small cell lung cancer. *Kaohsiung J Med Sci*. 2019; 35:151-159.

65. Kaira K, Higuchi T, Naruse I, Arisaka Y, Tokue A, Altan B et al. Metabolic activity by (18)F-FDG-PET/CT is predictive of early response after nivolumab in previously treated NSCLC. *Eur J Nucl Med Mol Imaging*. 2018; 45:56-66.

66. Evangelista L, Cuppari L, Menis J, Bonanno L, Reccia P, Frega S, Pasello G. 18F-FDG PET/CT in non-small-cell lung cancer patients: A potential predictive biomarker of response to immunotherapy. *Nucl Med Commun*. 2019; 40:802-807;

67. Seban RD, Mezquita L, Berenbaum A, Dercle L, Botticella A, Le Pechoux C et al. Baseline metabolic tumor burden on FDG PET/CT scans predicts outcome in advanced NSCLC patients treated with immune checkpoint inhibitors. *Eur J Nucl Med Mol Imaging*. 2020; 47:1147-1157.

68. Jreige M, Letovanec I, Chaba K, Renaud S, Rusakiewicz S, Cristina V et al. (18)F-FDG PET metabolic-to-morphological volume ratio predicts PD-L1 tumour expression and response to PD-1 blockade in non-small-cell lung cancer. *Eur J Nucl Med Mol Imaging*. 2019; 46:1859-1868.

69. Castello A, Carbone FG, Rossi S, Monterisi S, Federico D, Toschi L, Lopci E. Circulating Tumor Cells and Metabolic Parameters in NSCLC Patients Treated with Checkpoint Inhibitors. *Cancers*. 2020; 12:487.

70. Wang Y, Zhao N, Wu Z, Pan N, Shen X, Liu T et al. New insight on the correlation of metabolic status on (18)F-FDG PET/CT with immune marker expression in patients with non-small cell lung cancer. *Eur J Nucl Med Mol Imaging*. 2020; 47:1127-1136.

71. Im HJ, Pak K, Cheon GJ, Kang KW, Kim SJ, Kim IJ et al. Prognostic value of volumetric parameters of (18)F-FDG PET in non-small-cell lung cancer: a meta-analysis. *Eur J Nucl Med Mol Imaging*. 2015; 42:241-51.

72. Evangelista L, Cuocolo A, Pace L, Mansi L, Del Vecchio S, Miletto P, Sanfilippo S, Pellegrino S et al. Performance of FDG-PET/CT in solitary pulmonary nodule based on pre-test likelihood of malignancy: results from the ITALIAN retrospective multicenter trial. *Eur J Nucl Med Mol Imaging.* 2018; 45:1898-1907.

73. McWilliams A, Tammemagi M, Mayo JR, Roberts H, Liu G, Soghrati K et al. Probability of cancer in pulmonary nodules detected on first screening CT. *N Engl J Med*. 2013; 396:910-9.

74. Callister MEJ, Baldwin D, Akram AR et al. British Thoracic Society guidelines for the investigation and management of pulmonary nodules. *Thorax*. 2015; 70:i1–ii54.

75. Fonti R, Pellegrino S, Catalano L, Pane F, Del Vecchio S, Pace L. Visual and volumetric parameters by 18F-FDG-PET/CT: a head to head comparison for the prediction of outcome in patients with multiple myeloma. *Ann Hematol*. 2020; 99(1):127-135.

76. Barrington SF, Kluge R. FDG PET for therapy monitoring in Hodgkin and non-Hodgkin lymphomas. Eur J Nucl Med Mol Imaging. 2017; 44:97-110;

77. Salvatore B, Fonti R, De Renzo A, Pellegrino S, Ferrara IL, Mainolfi CG et al. 2-deoxy-2-[18F]fluoro-D-glucose positron emission tomography/computed tomography in primary extranodal lymphomas: treatment response evaluation and prognosis. Q J Nucl Med Mol Imaging. 2020; 64(2):219-225.

78. Cheson BD, Fisher RI, Barrington SF, Cavalli F, Schwartz LH, Zucca E et al. Recommendations for Initial Evaluation, Staging, and Response Assessment of Hodgkin and Non-Hodgkin Lymphoma: The Lugano Classification. *J Clin Oncol.* 2014; 32:3059-3068.

79. Itti E, Meignan M, Berriolo-Riedinger A et al. An international confirmatory study of the prognostic value of early PET/CT in diffuse large B- cell lymphoma: comparison between Deauville criteria and ΔSUVmax. *Eur J Nucl Med Mol Imaging*. 2013; 40:1312-1320.

80. Segreto S, Fonti R, Ottaviano M, Pellegrino S, Pace L, Damiano V, Palmieri G, Del Vecchio S. Evaluation of metabolic response with 18F-FDG PET-CT in patients with advanced or recurrent thymic epithelial tumors. *Cancer Imaging*. 2017; 17:10.

81. Lovinfosse P, Janvary ZJ, Coucke P, Jodogne S, Bernard C, Hatt M et al. FDG PET/CT texture analysis for predicting the outcome of lung cancer treated by stereotactic body radiation therapy. *Eur J Nucl Med Mol Imaging*. 2016; 43:1453-1460.

82. Bundschuh RA, Dinges J, Neumann L, Seyfried M, Zsótér M, Papp L et al. Textural Parameters of Tumor Heterogeneity in 18F-FDG PET/CT for Therapy Response Assessment and Prognosis in Patients with Locally Advanced Rectal Cancer. *J Nucl Med*. 2014; 55:891-897.

83. Hansell DM, Bankier A, MacMahon H, MacMahon H, McLoud TC, Muller NL et al. Fleischner society: glossary of terms for thoracic imaging 1. *Radiology*. 2008; 246:697-722.

84. Sim YT, Goh Y, Dempsey MF, Han S, Poon FW. PET-CT evaluation of solitary pulmonary nodules: correlation with maximum standardized uptake value and pathology. *Lung*. 2013; 191:625-32.

85. van Gómez López O, García Vicente AM, Honguero Martínez AF, Jiménez Londoño GA, Vega Caicedo CH, León Atance P, Soriano Castrejón ÁM. 18F-FDG-PET/CT in the assessment of pulmonary solitary nodules: comparison of different analysis methods and risk variables in the prediction of malignancy. *Transl Lung Cancer Res*. 2015; 4:228-235.

86. Chantry A, Kazmi M, Barrington S, Goh V, Mulholland N, Streetly M, Lai M, Pratt G, British Society for Haematology G. Guidelines for the use of imaging in the management of patients with myeloma. *Br J Haematol*. 2017; 178:380-393.

87. Ripani D, Caldarella C, Za T, Pizzuto DA, Rossi E, De Stefano V, Giordano A. Prognostic significance of normalized FDG-PET parameters in patients with multiple myeloma undergoing induction chemotherapy and autologous hematopoietic stem cell

transplantation: a retrospective single-center evaluation. *Eur J Nucl Med Mol Imaging*. 2019; 46:116-128;

88. Kyle RA, Rajkumar SV. Criteria for diagnosis, staging, risk stratification and response assessment of multiple myeloma. *Leukemia.* 2009; 23:3-9.

89. Nanni C, Zamagni E, Versari A, Chauvie S, Bianchi A, Rensi M et al. Image interpretation criteria for FDG PET/CT in multiple myeloma: a new proposal from an Italian expert panel. IMPeTUs (Italian Myeloma criteria for PET USe). *Eur J Nucl Med Mol Imaging*. 2016; 43:414-421.

90. Nanni C, Versari A, Chauvie S, Bertone E, Bianchi A, Rensi M et al. Interpretation criteria for FDG PET/CT in multiple myeloma (IMPeTUs): final results. IMPeTUs (Italian myeloma criteria for PET USe). *Eur J Nucl Med Mol Imaging*. 2018; 45:712-719.

91. Barrington SF, Mikhaeel NG, Kostakoglu L et al. The role of imaging in the staging and response assessment of lymphoma: consensus of the ICML Imaging Working Group. *J Clin Oncol*. 2014; 32(27):3048-3058.

92. Young H, Baum R, Cremerius U et al. Measurement of clinical and subclinical tumour response using [18F]-fluorodeoxyglucose and positron emission tomography: review and 1999 EORTC recommendations. European Organization for Research and Treatment of Cancer (EORTC) PET Study Group. *Eur J Cancer*. 1999; 35(13):1773-1778.

93. Minamimoto R, Fayad L, Advani R et al. Diffuse Large B-Cell Lymphoma: prospective multicenter comparison of early interim FLT PET/CT versus FDG PET/CT with IHP, EORTC, Deauville and PERCIST criteria for early therapeutic monitoring. *Radiology*. 2016; 280(1):220-9.

94. Campo E, Swerdlow SH, Harris NL, Pileri S, Stein H et Jaffe ES. The 2008 WHO Classification of Lymphoid Neoplasm and beyond: evolving concepts and practical applications. *Blood*. 2011; 117(19):5019-5032.

95. Zhou C, Duan X, Lan B, Liao J et Shen J. Prognostic CT and MR imaging features in patients with untreated extranodal non-Hodgkin lymphoma of the head and neck region. *Eur Radiol*. 2015; 25(10):3035-3042.

96. Vannata B, Zucca E. Primary extranodal B-cell lymphoma: current concepts and treatment strategies. *Chin Clin Oncol*. 2015; 4(1):10.

97. Paes FM, Kalkanis DG, Sideras PA et Serafini AN. FDG PET/CT of extranodal involvement in Non-Hodgkin Lymphoma and Hodgkin Disease. *RadioGraphics*. 2010; 30(1):269-291.

98. Martelli M, Ceriani L, Zucca E et al. 18F-Fluorodeoxyglucose positron emission tomography predicts survival after chemoimmunoterapy for primary mediastinal large B-cell lymphoma: results of the international extranodal lymphoma study group IELSG-26 study. *J Clin Oncol*. 2014; 32(17):1769-1775.

99. Lin C, Itti E, Haioun C et al. Early 18F-FDG PET for prediction of prognosis in patients with diffuse large B-cell lymphoma: SUV-based assessment versus visual analysis. *J Nucl Med*. 2007; 48(10):1626-1632.

100. Coughlan M, Elstrom R. The use of FDG-PET in diffuse large B cell lymphoma (DLBCL): predicting outcome following first line therapy. *Cancer Imaging*. 2014; 29;14-34.

101. Nagle SJ, Chong EA, Chekol S et al. The role of FDG-PET imaging as a prognostic marker of outcome in primary mediastinal B-cell lymphoma. *Cancer Med*. 2015; 4(1):7-15.

102. Srirajaskanthan R, Toubanakis C, Dusmet M, Caplin ME. A review of thymic tumours. *Lung Cancer.* 2008; 60:4-13.

103. Priola AM, Priola SM. Imaging of thymus in myasthenia gravis: from thymic hyperplasia to thymic tumor. *Clin Radiol*. 2014; 69:e230-45.

104. De Luca S, Fonti R, Palmieri G, Federico P, Del Prete G, Pacelli R, et al. Combined imaging with 18F-FDG-PET/CT and 111In-labeled octreotide SPECT for evaluation of thymic epithelial tumors. *Clin Nucl Med*. 2013; 38:354-8.

105. Sung YM, Lee KS, Kim BT, Choi JY, Shim YM, Yi CA. 18F-FDG PET/CT of thymic epithelial tumors: usefulness for distinguishing and staging tumor subgroups. *J Nucl Med*. 2006; 47:1628-34.

106. Endo M, Nakagawa K, Ohde Y, Okumura T, Kondo H, Igawa S et al. Utility of 18FDG-PET for differentiating the grade of malignancy in thymic epithelial tumors. *Lung Cancer*. 2008; 61:350-5.

107. Nakajo M, Kajiya Y, Tani A, Yoneda S, Shirahama H, Higashi M et al. (1)(8)FDG PET for grading malignancy in thymic epithelial tumors: significant differences in (1)(8)FDG uptake and expression of glucose transporter-1 and hexokinase II between low and high-risk tumors: preliminary study. *Eur J Radiol*. 2012; 81:146-51.

108. Park SY, Cho A, Bae MK, Lee CY, Kim DJ, Chung KY. Value of 18F-FDG PET/ CT for Predicting the World Health Organization Malignant Grade of Thymic Epithelial Tumors: Focused in Volume-Dependent Parameters. *Clin Nucl Med*. 2016; 41:15-20.

109. Benveniste MF, Moran CA, Mawlawi O, Fox PS, Swisher SG, Munden RF et al. FDG PET-CT aids in the preoperative assessment of patients with newly diagnosed thymic epithelial malignancies. *J Thorac Oncol*. 2013; 8:502-10.

110. Terzi A, Bertolaccini L, Rizzardi G, Luzzi L, Bianchi A, Campione A et al. Usefulness of 18-F FDG PET/CT in the pre-treatment evaluation of thymic epithelial neoplasms. *Lung Cancer*. 2011; 74:239-43.

111. Viti A, Terzi A, Bianchi A, Bertolaccini L. Is a positron emission tomography-computed tomography scan useful in the staging of thymic epithelial neoplasms? *Interact Cardiovasc Thorac Surg*. 2014; 19:129-34.

112. Thomas A, Mena E, Kurdziel K, Venzon D, Khozin S, Berman AW et al. 18F-fluorodeoxyglucose positron emission tomography in the management of patients with thymic epithelial tumors. *Clin Cancer Res*. 2013; 19:1487-93.

113. Strosberg J, El-Haddad G, Wolin E et al. Phase 3 trial of 177Lu-Dotatate for midgut neuroendocrine tumors. *N Engl J Med*. 2017; 376:125-135.

114. Kong G, Hicks RJ. Peptide Receptor Radiotherapy: Current approaches and future directions. *Curr Treat Options Oncol*. 2019; 20:77.

115. Reubi JC, Waser B. Concomitant expression of several peptide receptors in neuroendocrine tumours: molecular basis for in vivo multireceptor tumour targeting. *Eur J Nucl Med Mol Imaging*. 2003; 30:781-793.

116. Qian ZR, Li T, Ter-Minassian M et al. Association between somatostatin receptor expression and clinical outcomes in neuroendocrine tumors. *Pancreas.* 2016; 45:1386-1393.

117. Hu Y, Ye Z, Wang F et al. Role of somatostatin receptor in pancreatic neuroendocrine tumor development, diagnosis, and therapy. *Front Endocrinol*. 2021; 12:679000.

8 TABLES

Table 1. Volume-based imaging parameters derived from 18F-FDG PET/CT and expressed as mean±SE in NSCLC patients.

Parameter	No of patients	Mean ± SE	Range
MTV_{TOT}	65	81.83 ± 14.63	0.19–540.98
Primary tumors	65	31.45 ± 6.94	0.16–311.70
Regional nodes	27	78.17 ± 25.17	0.36–531.61
Distant metastases	29	40.15 ± 9.88	0.42–220.85
TLG_{WB}	65	459.88 ± 77.02	0.44–2524.06
Primary tumors	65	198.64 ± 41.34	0.44–1382.30
Regional nodes	27	381.85 ± 108.71	0.99–2196.49
Distant metastases	29	230.04 ± 59.56	1.38–1364.24

MTV_{TOT} total metabolic tumor volume, *TLG_{WB}* whole-body total lesion glycolysis

Adapted by permission from: Pellegrino S, Fonti R, Mazziotti E, Piccin L, Mozzillo E, Damiano V, Matano E, De Placido S, Del Vecchio S. Total metabolic tumor volume by 18F-FDG PET/CT for the prediction of outcome in patients with non-small cell lung cancer. *Ann Nucl Med*. 2019; 33:937–944.

Table 2. Predictors of PFS and OS by univariate analysis of clinical and imaging variables in NSCLC patients.

Variable	Progression-free survival		Overall survival	
	χ^2	p	χ^2	p
Age	1.7910	0.1808	3.6670	0.0550
Gender	0.0271	0.8692	0.3870	0.5340
Primary tumor diameter	3.9440	0.0470	2.7060	0.0990
Histology	0.2340	0.6286	0.3770	0.5391
Primary tumor SUV_{max}	1.1040	0.2935	0.3340	0.5635
Primary tumor MTV	4.7130	0.0299	4.3260	0.0375
Primary tumor TLG	2.7850	0.0951	2.2010	0.1380
MTV_{TOT}	12.9340	0.0003	14.9640	0.0001
TLG_{WB}	13.5490	0.0002	11.2520	0.0008
Stage	25.6290	<0.0001	23.3690	<0.0001
Treatment (surgery vs other)	21.2330	<0.0001	21.0400	<0.0001

SUV_{max} maximum standardized uptake value, *MTV* metabolic tumor volume, *TLG* total lesion glycolysis, *MTV_{TOT}* total metabolic tumor volume, *TLG_{WB}* whole-body total lesion glycolysis

Adapted by permission from: Pellegrino S, Fonti R, Mazziotti E, Piccin L, Mozzillo E, Damiano V, Matano E, De Placido S, Del Vecchio S. Total metabolic tumor volume by 18F-FDG PET/CT for the prediction of outcome in patients with non-small cell lung cancer. *Ann Nucl Med*. 2019; 33:937–944.

Table 3. Clinical studies evaluating the prognostic role of MTV and TLG determined in primary tumors of NSCLC patients.

Clinical Study	N° of Patients	TNM Stage	Endpoints	Volumetric Parameters	Threshold or Delineation Method	Determination of Cut-Off Value	Cut-Off Values MTV	Cut-Off Values TLG
Davison et al. (2013) [47]	39	I/IV	12 mo. Survival OS	MTV/TLG	gradient-based	median value ROC curve	9.7 mL 79 mL	74 g 349 g
Hyun et al. (2013) [40]	529	IA/IIB	OS/DFS	MTV/TLG	mediastinal background SUVavg plus its 2 SD	ROC curve	16 cm^3	70 g
Anwar et al. (2018) [48]	49	IA/IB	DFS	MTV/TLG	SUV (2.5)	ROC curve	6.6 mL	36.6 g
Dosani et al. (2019) [49]	134	inoperable IA/IB	LC OS	MTV/TLG	gradient-based	median value	2.4 mL	10.9 g
Yanarates et al. (2020) [50]	258	IIIB/IV	OS/PFS	MTV/TLG	50%SUVmax	ROC curve	5.7 mL	49.4 g
Kim et al. (2014) [51]	63	IA/IIB	OLM	MTV/TLG	SUV (2.5)	ROC curve	18.9 cm^3	88.4 g
Park et al. (2015) [52]	139	I	OLM	MTV/TLG	SUV (2.0)	ROC curve	3.055 mL	9.829 g
Roengvoraphoj et al. (2018) [53]	65	inoperable IIIA/IIIB	OS	MTV	50%SUVmax	pre-CRT post-CRT Δmid-CRT	63 cm^3 25 cm^3 ≥15%	- - -
Roengvoraphoj et al. (2018) [54]	60	inoperable IIIA/IIIB	OS	MTV	50%SUVmax	Δpost-CRT	≥80%	-

MTV metabolic tumor volume; TLG total lesion glycolysis; NSCLC non-small cell lung cancer; OS overall survival; ROC receiver operating characteristic; DFS disease free survival; SUV standardized uptake value; SD standard deviation; LC local control; PFS progression-free survival; OLM occult lymph node metastasis; CRT chemoradiotherapy.

Table 4. Clinical studies evaluating the prognostic role of whole-body MTV and whole-body TLG of NSCLC patients.

Clinical Study	N° of Patients	TNM Stage	Endpoints	Volumetric Parameters	Threshold or Delineation Method	Determination of Cut-Off Value	Cut-Off Values MTV	Cut-Off Values TLG
Bazan et al. (2017) [57]	230	inoperable IIB/IIIB	OS LC	MTV	60% adaptive threshold of the SUVpeak within each lesion	median value	32 mL	-
Finkle et al. (2017) [58]	330	IIB/IIIB	OS	MTV	gradient-based	Log-rank test	29.2 mL	-
Ventura et al. (2020) [59]	193	operable I/IV	OS	MTV/TLG	42%SUVmax	ROC curve	8.15 mL	21.85 g
Liao et al. (2012) [24]	169	inoperable II/IV	OS	MTV/TLG	gradient-based	tertiles	33.5 mL 134.9 mL 473.0 mL	107.3 g 504.0 g 1898.1 g
Pellegrino et al. (2019) [60]	65	I/IV	OS/PFS	MTV/TLG	SUV (2.5)	ROC curve	9.5 mL	54.7 g
Chen et al. (2012) [61]	105	I/IV	OS/PFS	TLG	50%SUVmax	ROC curve	-	655 g
Vanhove et al. (2018) [62]	105	I/IV	OS/PFS	MTV/TLG	50%SUVmax	median value	14.6 mL	93.4 g
Lapa et al. (2017) [63]	278	I/IV	OS	MTV	SUV (2.5)	R software	49.5 mL	-
Pu et al. (2018) [64]	935	I/IV	OS	MTV	gradient-based	quartiles	10 mL 53.4 mL 155 mL	- - -
Chin et al. (2018) [65]	55	oligometastatic I/IV	OS	MTV/TLG	gradient-based	quartiles (highest vs. remaining)	17.8 mL	86.8 g
Kong et al. (2019) [29]	102	inoperable I/III	OS	MTV/TLG	Auto-segmentation at tumor/aorta ratio of 1.5 followed by manual editing according to CT anatomy	median value after mid-RT with conventional RT or PET-adapted RT	41 mL 46 mL	- -
Chen et al. (2019) [66]	25	IIIA/IIIB	OS/PFS	MTV/TLG	50%SUVmax	Δmedian value after mid-RT	42%	65%
Xiao et al. (2017) [67]	17	II/III	RT adjustment based on ΔMTV	MTV	fixed source/background ratio combined with CT anatomy based manual editing	mean value pre-RT mean value during-RT	136.2 mL 64.7 mL	- -

MTV metabolic tumor volume; TLG total lesion glycolysis; NSCLC non-small cell lung cancer; OS overall survival; LC local control; SUV standardized uptake value; ROC receiver operating characteristic; PFS progression-free survival; CT computed tomography; RT radiotherapy; PET positron emission tomography.

From Pellegrino S, Fonti R, Pulcrano A, Del Vecchio S. PET-Based Volumetric Biomarkers for Risk Stratification of Non-Small Cell Lung Cancer Patients. *Diagnostics*. 2021; 11(2):210.

Table 5. Predictors of overall survival and progression-free survival by univariate analysis of clinical and imaging variables.

Variable	Overall survival		Progression-free survival	
	χ^2	P	χ^2	P
Age	1.2300	0.2673	0.0544	0.8155
Gender	0.3720	0.5418	1.7760	0.1826
Primary tumor diameter	0.0062	0.9374	0.0281	0.8668
Histology	1.6550	0.1982	2.0280	0.1545
SUVmax (≤ 11.63 vs > 11.63)	0.0767	0.7818	0.00001	0.9954
SUVmean (≤ 5.05 vs > 5.05)	1.2460	0.2643	1.1890	0.2755
COV (≤ 0.38 vs > 0.38)	5.5600	0.0184	2.3350	0.1265
Primary tumor MTV	0.3550	0.5515	0.7230	0.3951
Primary tumor TLG	0.0918	0.7619	0.2600	0.6099
MTV_{TOT}	7.8820	0.0050	8.0390	0.0046
TLG_{WB}	6.4920	0.0108	7.6680	0.0056
Stage	8.2530	0.0041	8.3320	0.0039

SUVmax: Maximum standardized uptake value; MTV: Metabolic Tumor Volume; TLG: Total Lesion Glycolysis; MTV_{TOT}: Total Metabolic Tumor Volume; TLG_{WB}: Whole body Total Lesion Glycolysis

Table 6. Visual IMPeTUs-based parameters obtained from 18F-FDG PET/CT scans in MM patients.

IMPeTUs criteria	Patients
5-PS of diffuse BM uptake	
Score 1	0
Score 2	9 (19%)
Score 3	25 (53%)
Score 4	12 (26%)
Score 5	1 (2%)
Diffuse BM uptake in limbs/ribs	37 (79%)
No. of focal lesions	
X_1 (None)	0
X_2 ($N = 1$ to 3)	23 (49%)
X_3 ($N = 4$ to 10)	16 (34%)
X_4 ($N > 10$)	8 (17%)
Site of focal lesions	
Skull	6 (13%)
Spine	29 (62%)
Extra spine	42 (89%)
5-PS of the hottest lesion	
Score 1	0
Score 2	1 (2%)
Score 3	0
Score 4	8 (17%)
Score 5	38 (81%)
No. of lytic lesions	
X_1 (None)	0
X_2 ($N = 1$ to 3)	26 (55%)
X_3 ($N = 4$ to 10)	14 (30%)
X_4 ($N > 10$)	7 (15%)
Fracture	0
Paramedullary	7 (15%)
Extramedullary	3 (6%)

5-PS, 5-point scale; *BM*, bone marrow

Adapted by permission from: Fonti R, Pellegrino S, Catalano L, Pane F, Del Vecchio S, Pace L. Visual and volumetric parameters by 18F-FDG-PET/CT: a head to head comparison for the prediction of outcome in patients with multiple myeloma. *Ann Hematol*. 2020; 99(1):127-135.

9 FIGURES

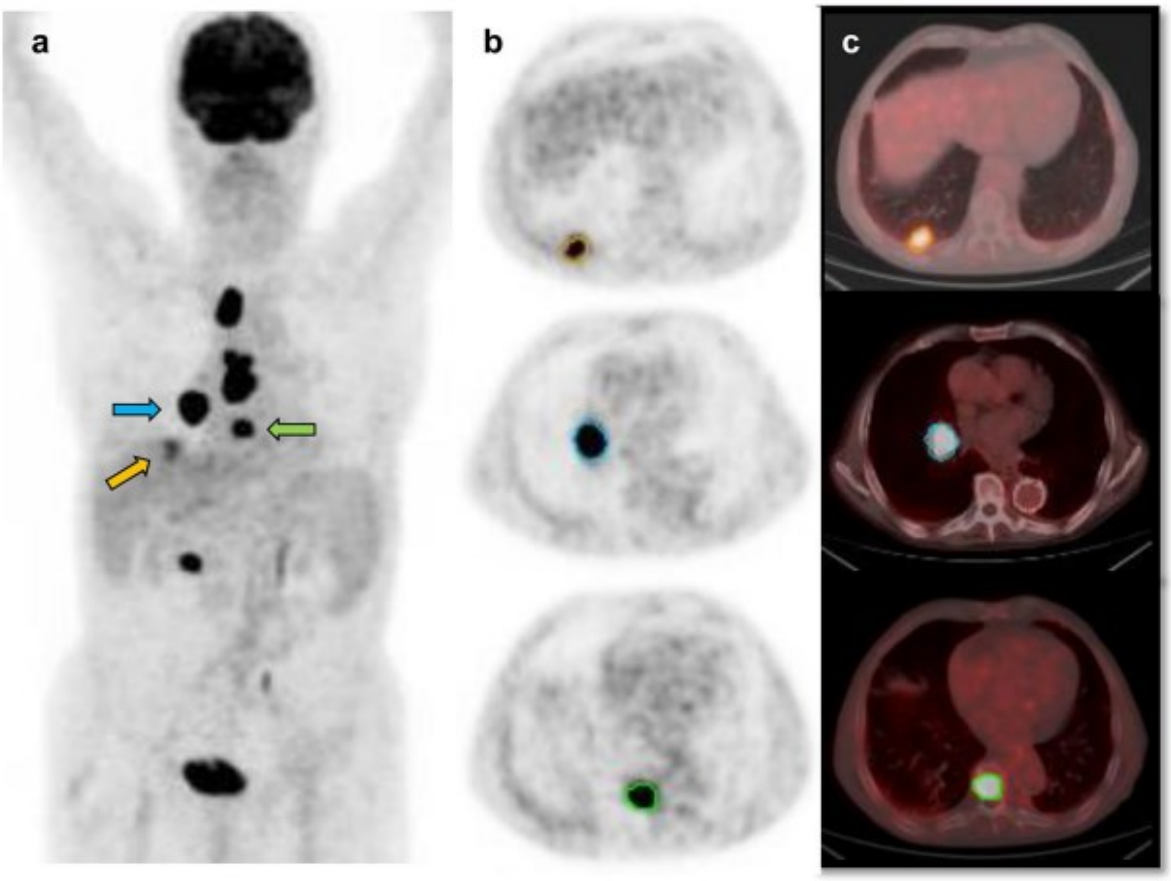

Figure 1. Representative images of 18F-FDG PET/CT study in a 74-year-old patient with stage IVA lung adenocarcinoma. Panel **a** shows the maximal intensity projection image with arrows indicating primary tumor (orange), lymph node metastasis (blue) and bone metastasis (green). Panel **b** and **c** show transaxial PET images and fusion images of co-registered PET and CT. Tridimensional regions of interest were drawn around primary tumor, lymph node metastases and bone lesion and segmentation was performed using an automated contouring program setting a threshold for SUVmax at 2.5. Examples of segmentation of primary lung tumor (orange), lymph node metastasis (blue) and bone metastasis (green) are provided in panels **b** and **c**. MTV_{TOT} was 95.68 ml and TLG_{WB} was 760.13 g; OS of this patient was 3 months. Adapted by permission from: Pellegrino S, Fonti R, Mazziotti E, Piccin L, Mozzillo E, Damiano V, Matano E, De Placido S, Del Vecchio S. Total metabolic tumor volume by 18F-FDG PET/CT for the prediction of outcome in patients with non-small cell lung cancer. *Ann Nucl Med*. 2019; 33:937-944.

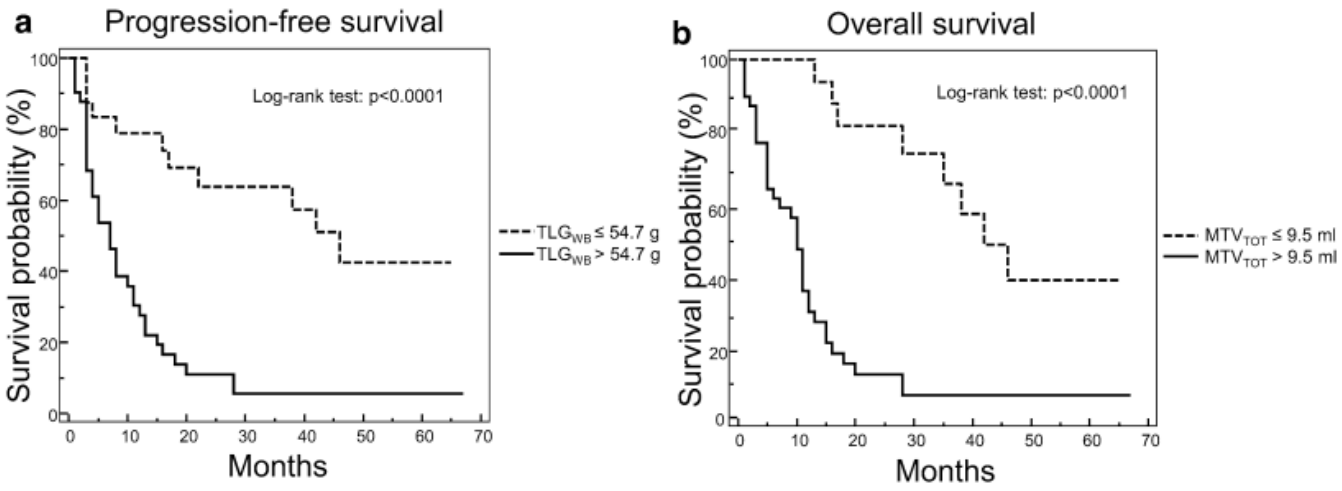

Figure 2. Survival analysis in 65 NSCLC patients.

a PFS was evaluated by Kaplan-Meier analysis and log-rank test in 65 patients with NSCLC using a cutoff of 54.7 g for TLG_{WB} as determined by ROC curve analysis. Patients with TLG_{WB} lower than the cutoff had a significantly prolonged PFS as compared to that of patients with TLG_{WB} higher than the cutoff (χ^2=19.5414, p<0.0001).

b OS was evaluated by Kaplan-Meier analysis and log-rank test in 65 patients with NSCLC using a cutoff of 9.5 ml for MTV_{TOT} as determined by ROC curve analysis. Patients with MTV_{TOT} lower than 9.5 ml had a significantly better OS than that of patients with MTV_{TOT} higher than the cutoff (χ^2=16.8284, p<0.0001). Adapted by permission from: Pellegrino S, Fonti R, Mazziotti E, Piccin L, Mozzillo E, Damiano V, Matano E, De Placido S, Del Vecchio S. Total metabolic tumor volume by 18F-FDG PET/CT for the prediction of outcome in patients with non-small cell lung cancer. *Ann Nucl Med*. 2019; 33:937–944.

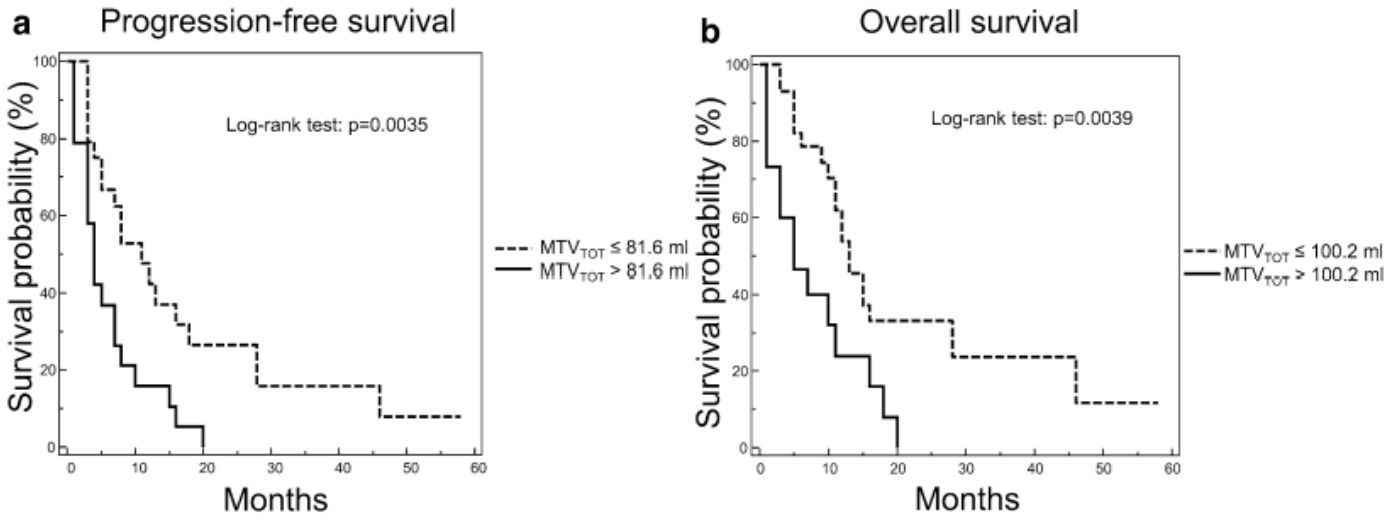

Figure 3. Survival analysis in 43 NSCLC patients (out of 65) with advanced disease (stages III and IV).

a Survival analysis by Kaplan-Meier method and log-rank testing showed that patients with $MTV_{TOT} \leq 81.6$ ml had a PFS significantly prolonged than that of patients with a $MTV_{TOT} > 81.6$ ml ($\chi^2=8.5297$, p=0.0035).

b OS was significantly better in patients with a $MTV_{TOT} \leq 100.2$ ml as compared to those with $MTV_{TOT} > 100.2$ ml ($\chi^2=8.3283$, p=0.0039). Adapted by permission from: Pellegrino S, Fonti R, Mazziotti E, Piccin L, Mozzillo E, Damiano V, Matano E, De Placido S, Del Vecchio S. Total metabolic tumor volume by 18F-FDG PET/CT for the prediction of outcome in patients with non-small cell lung cancer. *Ann Nucl Med*. 2019; 33:937–944.

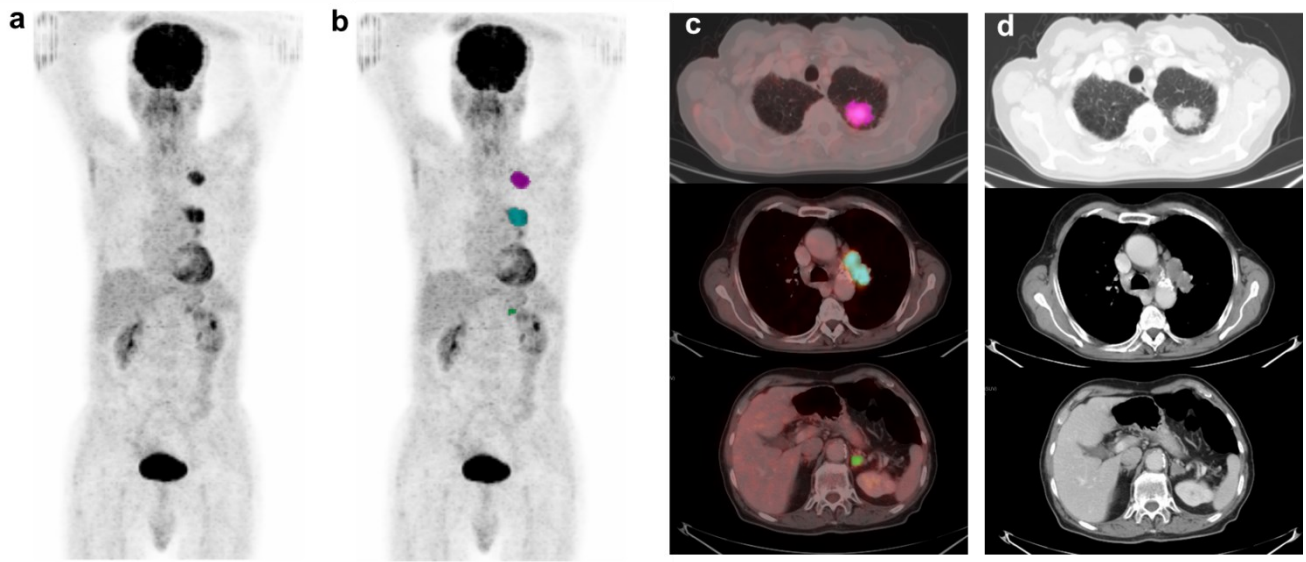

Figure 4. Representative images of 18F-FDG PET/CT scan in a 80-year-old patient with stage IVA non-small cell lung cancer.

Maximal intensity projection images are shown in panel **a** and **b**. Transaxial fusion images of co-registered PET/CT and CT images are shown in panels **c** and **d**. Tridimensional regions of interest were drawn around primary tumor, lymph node metastasis and adrenal lesion and segmentation was performed using an automated contouring program setting a threshold for SUVmax at 2.5. Examples of segmentation of primary lung tumor (pink), lymph node (light blue) and adrenal metastasis (green) are provided in panels **c** and **d**. CoV of primary lung tumor was 0.25 and MTV_{TOT} was 42.67 ml; OS of this patient was 10 months.

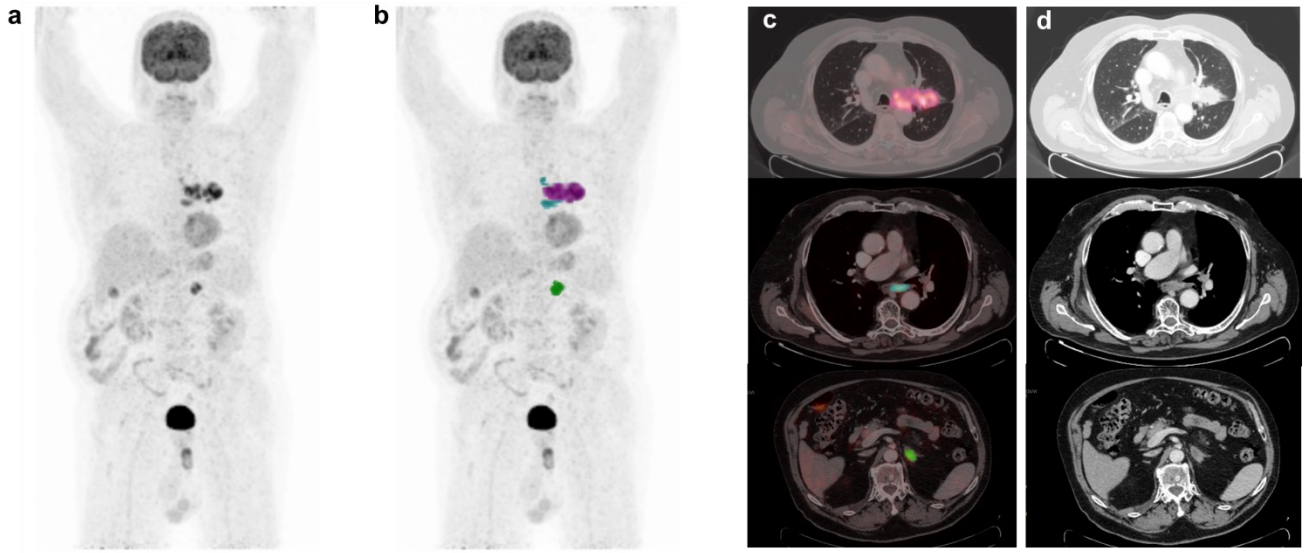

Figure 5. Representative images of 18F-FDG PET/CT scan in a 72-year-old patient with stage IVA non-small cell lung cancer.

Maximal intensity projection images are shown in panel **a** and **b**. Transaxial fusion images of co-registered PET/CT and CT images are shown in panels **c** and **d**. Tridimensional regions of interest were drawn around primary tumor, lymph node metastases and adrenal lesion and segmentation was performed using an automated contouring program setting a threshold for SUVmax at 2.5. Examples of segmentation of primary lung tumor (pink), lymph node (light blue) and adrenal metastasis (green) are provided in panels **c** and **d**. CoV of primary lung tumor was 0.52 and MTV_{TOT} was 107.07 ml; this patient was still alive after 10 months of follow-up.

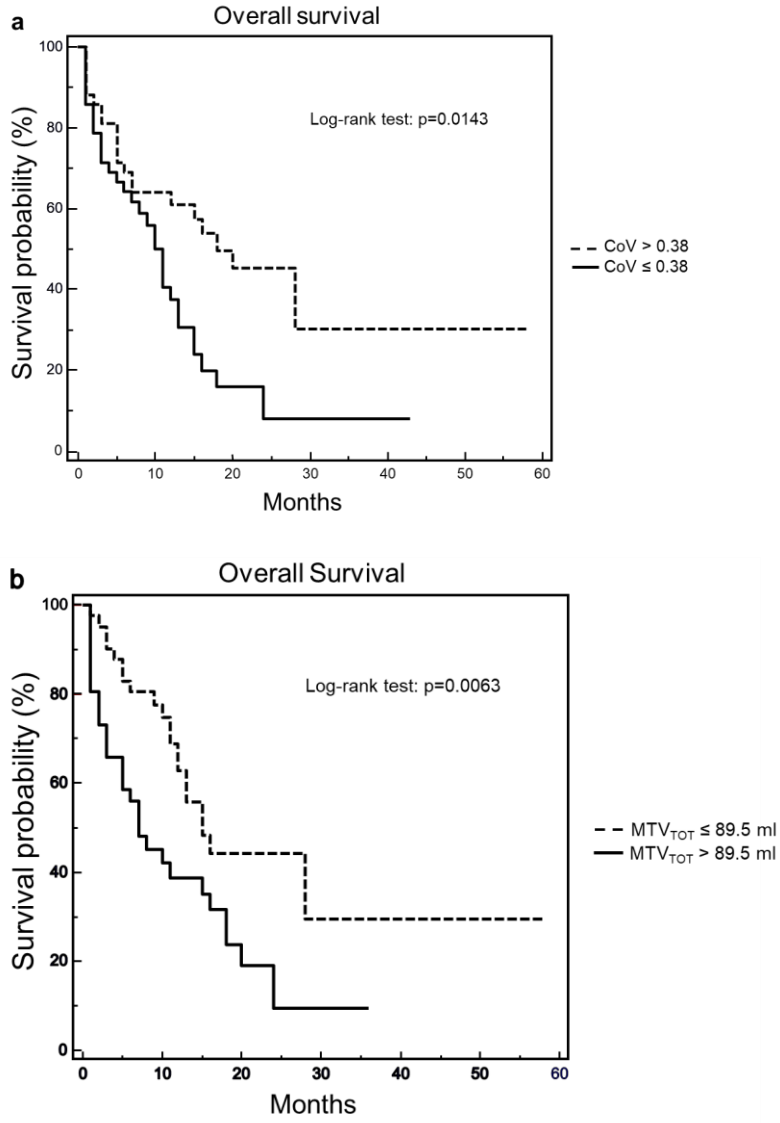

Figure 6. Survival analysis for OS in 84 patients with advanced NSCLC (stages III and IV). **a** OS was evaluated by Kaplan-Meyer analysis and log-rank test in 84 patients with NSCLC in advanced disease (stages III and IV) using the median value of 0.38 as cutoff for CoV. Patients with CoV > 0.38 showed significantly better OS than those having CoV ≤ 0.38 (χ^2=6.0005, p=0.0143).

b OS was evaluated by Kaplan-Meyer analysis and log-rank test in 84 patients with NSCLC in advanced disease (stages III and IV) using the median value of 89.5 ml for MTV_{TOT}. Patients with MTV_{TOT} ≤ 89.5 ml showed significantly better OS than those having MTV_{TOT} > 89.5 ml (χ^2=7.4546, p=0.0063).

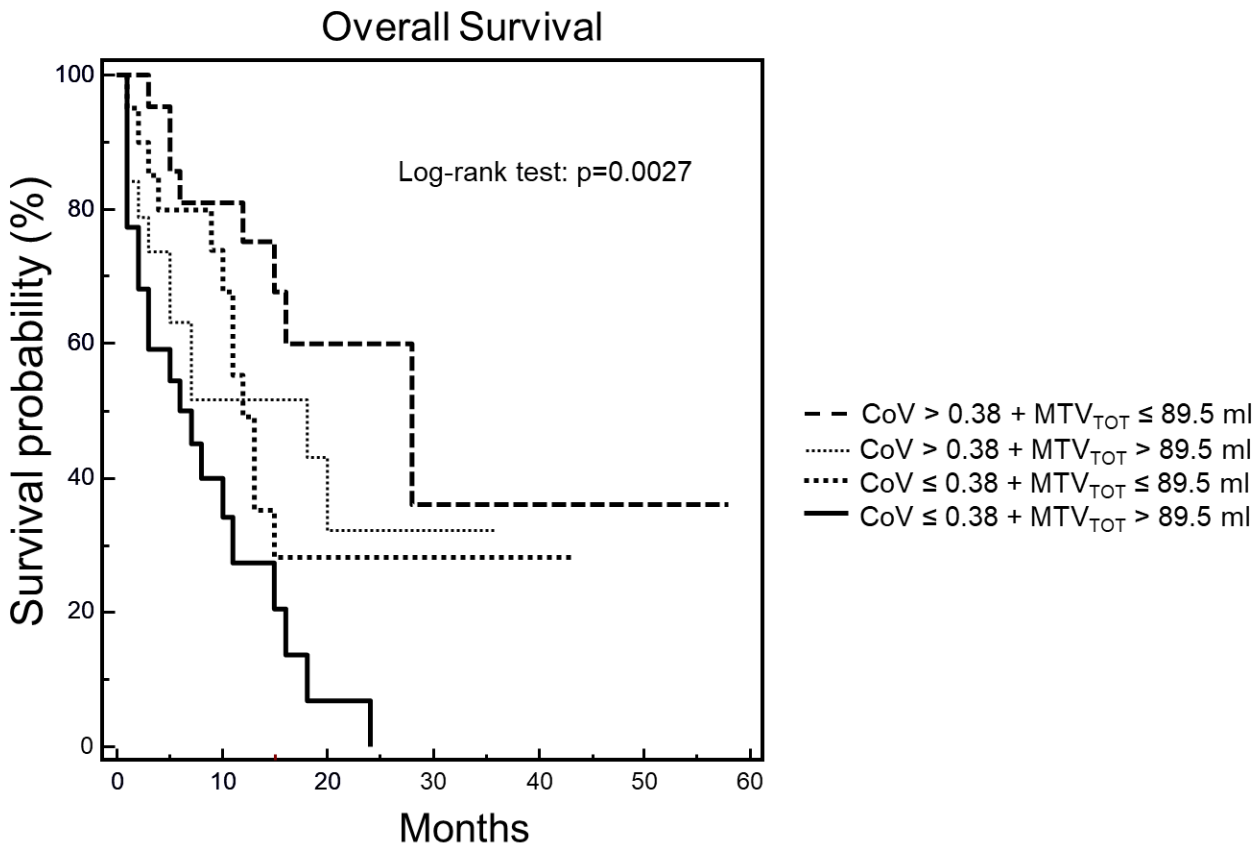

Figure 7. Combined model for overall survival analysis in 84 patients with advanced NSCLC (stages III and IV).

OS was evaluated by Kaplan-Meyer analysis and log-rank test in 84 patients with NSCLC in advanced disease (stages III and IV) using the cutoff of 0.38 for CoV and 89.5 ml for MTV_{TOT}. There was a statistically significant difference among the four survival curves (χ^2=14.1719, p=0.0027). Patients with COV ≤ 0.38 and MTV_{TOT} > 89.5 ml had the worst OS whereas patients with CoV > 0.38 and MTV_{TOT} ≤ 89.5 ml showed the best OS.

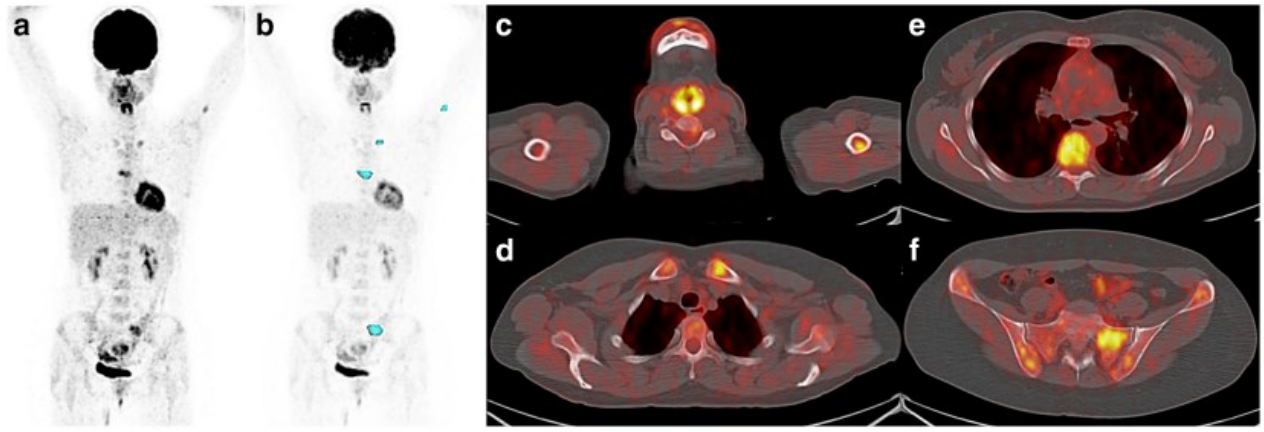

Figure 8. Representative images of 18F-FDG PET/CT scan showing visual and volumetric parameters obtained in a 54-year-old MM patient.

a Maximal intensity projection image.

b Maximal intensity projection view with overlay of segmented MTV of all myeloma lesions (MTV = 29.8 ml; TLG = 75.6 g).

c, d, e, f Transaxial fused images. In this MM patient visual parameters were as follows: diffuse bone marrow uptake according to 5-PS Deauville scale: score 4; presence of focal PET-positive lesions in the spine (**e**) and extra spine: left humerus (**c**), left clavicle (**d**), and sacrum (**f**); n.4 focal PET-positive lesions; metabolic state of the hottest lesion (**e**) according to the Deauville 5-PS: score 5; n.3 lytic lesions (**d-f**). Adapted by permission from: Fonti R, Pellegrino S, Catalano L, Pane F, Del Vecchio S, Pace L. Visual and volumetric parameters by 18F-FDG-PET/CT: a head to head comparison for the prediction of outcome in patients with multiple myeloma. *Ann Hematol*. 2020; 99(1):127-135.

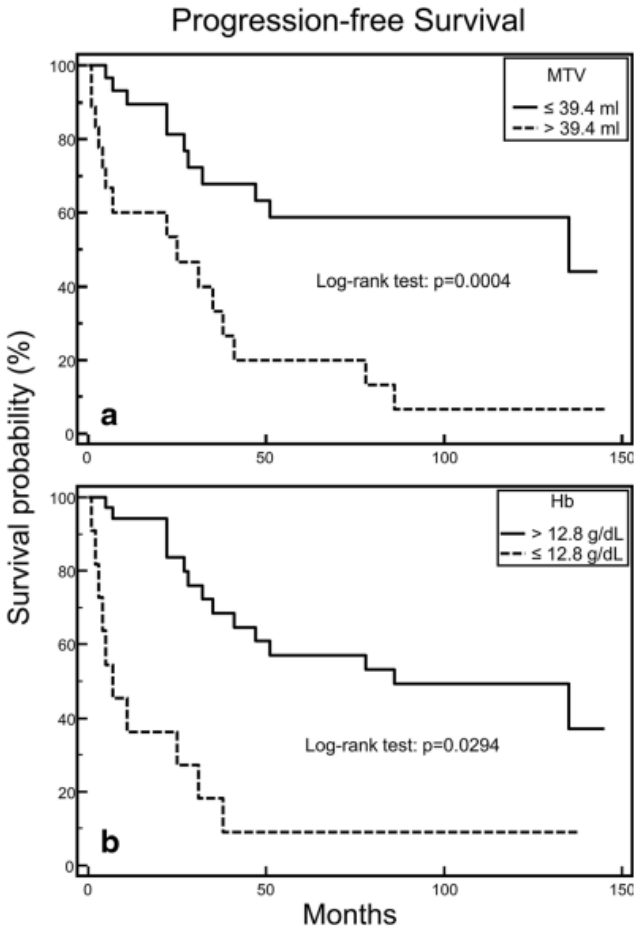

Figure 9. Progression-free survival by Kaplan-Meier analysis and log-rank test after 150-month follow-up in 47 MM patients.

a Statistically significant difference in PFS between MM patients with MTV values lower or higher than the cutoff level of 39.4 ml, as assessed by the ROC curve analysis (p=0.0004).

b Statistically significant difference in PFS between MM patients with hemoglobin levels lower or higher than the median value 12.8 g/dL (p=0.0294). Adapted by permission from: Fonti R, Pellegrino S, Catalano L, Pane F, Del Vecchio S, Pace L. Visual and volumetric parameters by 18F-FDG-PET/CT: a head to head comparison for the prediction of outcome in patients with multiple myeloma. *Ann Hematol*. 2020; 99(1):127-135.

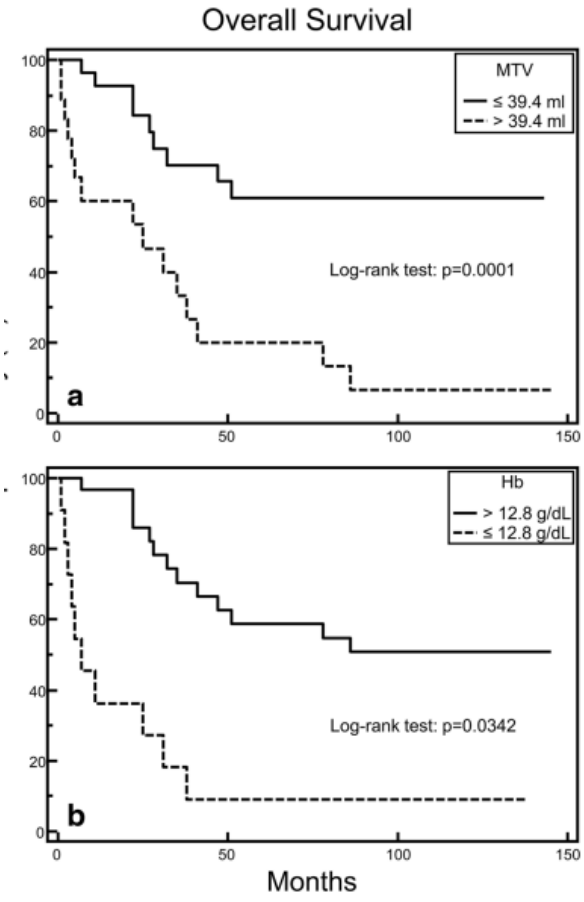

Figure 10. Overall survival by Kaplan-Meier analysis and log-rank test at 150-month follow-up in 47 MM patients.

a Statistically significant difference in OS between MM patients with MTV values lower or higher than the cutoff level of 39.4 ml, as assessed by the ROC curve analysis (p=0.0001). **b** Statistically significant difference in OS between MM patients with hemoglobin levels lower or higher than the median value 12.8 g/dL (p=0.0342). Adapted by permission from: Fonti R, Pellegrino S, Catalano L, Pane F, Del Vecchio S, Pace L. Visual and volumetric parameters by 18F-FDG-PET/CT: a head to head comparison for the prediction of outcome in patients with multiple myeloma. *Ann Hematol*. 2020; 99(1):127-135.

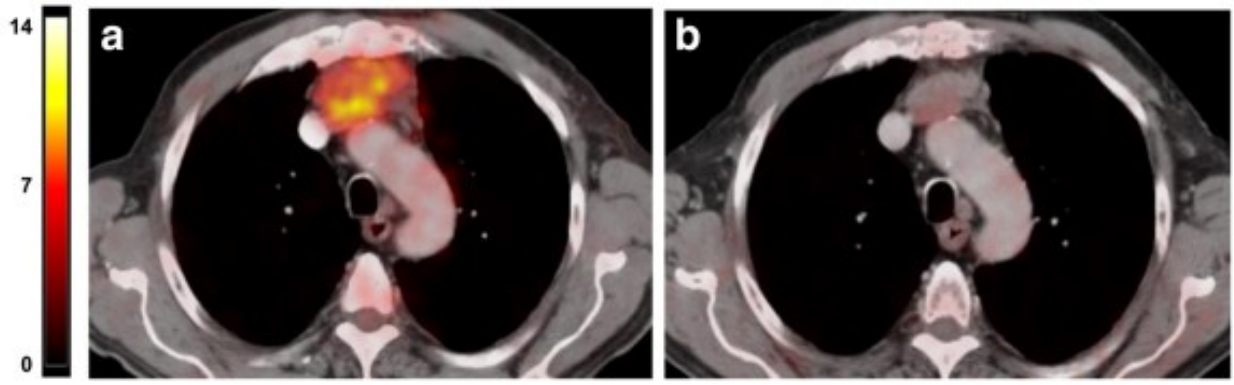

Figure 11. Representative images of baseline (**a**) and post-treatment (**b**) 18F-FDG PET/CT study in a patient with thymic carcinoma**.**

Fusion images of co-registered transaxial 18F-FDG PET and contrast-enhanced CT sections are shown in panels **a** and **b.** In the baseline study SUVmax was 6.60 whereas the post-treatment scan showed a SUVmax of 3.50. A 47% reduction of 18F-FDG uptake was found in this patient with partial response (PR) based on RECIST. The same maximum threshold of SUV was applied to PET images from pre-treatment and post-treatment scans as shown by the color scale on the left of the figure. From Segreto S, Fonti R, Ottaviano M, Pellegrino S, Pace L, Damiano V, Palmieri G, Del Vecchio S. Evaluation of metabolic response with 18F-FDG PET-CT in patients with advanced or recurrent thymic epithelial tumors. *Cancer Imaging*. 2017; 17:10.

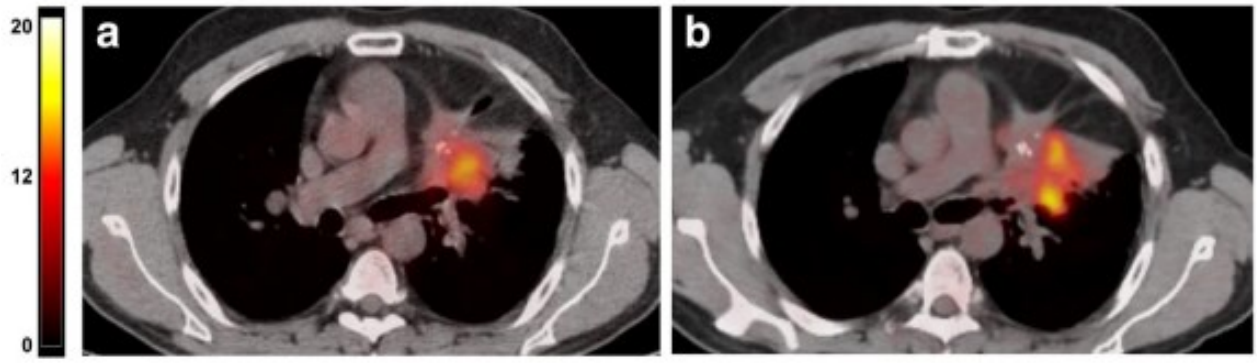

Figure 12. Representative images of baseline (**a**) and post-treatment (**b)** 18F-FDG PET-CT study in a patient with thymic carcinoma.

Fusion images of co-registered transaxial 18F-FDG PET and CT sections are shown in panels **a** and **b**. In the baseline study SUVmax was 8.80 whereas the post-treatment study showed a SUVmax of 14.40. A 64% increase of 18F-FDG uptake was found in this patient with stable disease (SD) based on RECIST. The same maximum threshold of SUV was applied to PET images from pre-treatment and post-treatment scans as shown by the color scale on the left of the figure. From Segreto S, Fonti R, Ottaviano M, Pellegrino S, Pace L, Damiano V, Palmieri G, Del Vecchio S. Evaluation of metabolic response with 18F-FDG PET-CT in patients with advanced or recurrent thymic epithelial tumors. *Cancer Imaging*. 2017; 17:10.